Distribution of Higher-Order Structures in Injection Moldings of Particulate-Filled Polypropylenes

MITSUYOSHI FUJIYAMA* and TETSUO WAKINO

Polymer Development Laboratory, Tokuyama Soda Co., Ltd., Tokuyama-shi, Yamaguchi-ken 745, Japan

SYNOPSIS

Flexural test specimens were injection-molded from polypropylenes filled with flaky talc or spherical calcium carbonate at levels of 0–40 wt % under cylinder temperatures of 200–320°C. Distributions in the flow direction of higher-order structures such as thickness of skin layer, a^*-axis-oriented component fraction $[A^*]$, and crystalline orientation functions and distributions in the thickness direction of higher-order structures such as crystallinity, β-crystal content, $[A^*]$, and crystalline orientation functions were studied. These higher-order structures are inhomogeneous in the flow and thickness directions also for injection moldings of particulate-filled polypropylenes, which strongly influences the product properties such as mechanical and thermal properties. Molecular orientation process in injection molding was theoretically analyzed from a viewpoint of growth of recoverable shear strain at the gate and its relaxation in the cavity, which could considerably well explain the influences of particulate filling and cylinder temperature on not only the mean values but also the changes in the flow and thickness directions, of the quantities such as thickness of the skin layer and crystalline orientation functions, which express the degree of molecular orientation.

INTRODUCTION

In injection molding of thermoplastics, since molten resin solidifies under inhomogeneous stress and cooling conditions, the inner structures of the molded article are inhomogeneous, influencing the product properties. Consequently, it is important in injection molding technology of thermoplastics to clarify the influences of the primary structures of resin and molding conditions on the inhomogeneous structure of the molded article.

Many studies have so far been carried out on the distributions of higher-order structures in injection moldings of unfilled plastics. However, as for the injection moldings of filled plastics, concern has been focused mainly on the orientation of fibers in fiber-filled plastics such as glass or carbon fiber-filled plastics, and studies on the higher-order structures of matrix resin are not so many.[1–12] Folks and Russell[1] injection-molded rectangular plates from glass fiber-filled polypropylene and high density polyethylene by varying injection speed, measured the orientation state of glass fibers and the degree of molecular orientation, and found that glass fibers scarcely influenced the degree of molecular orientation of matrix resin at glass fiber contents of commercial use level and the degree of molecular orientation was governed by the orientation of glass fibers at higher glass fiber contents. Xavier et al.[2] observed skin/core structures in injection moldings of a glass fiber-filled polypropylene and found that the skin layer was thicker as injection pressure and injection speed were higher and cylinder temperature was lower. Xavier and Misra[3] injection-molded tensile test specimens from polypropylenes with various glass fiber contents and found that the skin/core structure became obscure and at the same time the skin layer became thinner with increasing glass fiber content and that the skin/core structure vanished at glass fiber contents of 35 wt % or more. Xavier and Sharma[6] observed skin/core structures in injection moldings of mica-filled polypropylenes and found that the skin layer became very thin even at

* To whom correspondence should be addressed.

Journal of Applied Polymer Science, Vol. 43, 97–128 (1991)
 CCC 0021-8995/91/010097-32$04.00

a mica content of 10 wt % in comparison with unfilled polypropylene injection molding, became thinner at mica contents of 20 wt % or more, and could not be observed at mica contents of 40 wt % or more. The authors[10] injection-molded flexural test specimens from polypropylenes filled with talc or calcium carbonate and found that the thickness of the skin layer and the degree of crystalline orientation decreased with increasing cylinder temperature and increased with increasing filler content compared at the same cylinder temperature. The authors[10] also showed that product properties such as flexural modulus, flexural strength, and mold shrinkage decreased with increasing cylinder temperature and that rectilinear relationships existed between the product properties and the thickness of the skin layer or the degree of crystalline orientation at each filler content level. Furthermore, the authors[11] theoretically analyzed molecular orientation process in injection molding from a viewpoint of growth of a melt orientation (recoverable shear strain) at the gate and its relaxation in the cavity and showed that the increases of the thickness of the skin layer and the degree of crystalline orientation by the filling of particulates were caused by (i) long relaxation time of recoverable shear strain, (ii) high thermal diffusivity, and (iii) high crystallization temperature. Morales and White[12] observed skin/core structures in injection moldings of spiolite- or talc-filled polypropylenes and showed that the thickness of the skin layer increased and the boundary between the skin and core layers became obscure with increasing filler content as in the case of the authors' results. They also showed from infrared dichroism measurements that the degrees of the crystalline and mean molecular orientations of the skin layer decreased with increasing filler content. Further, the formation of transcrystals around fillers in injection moldings of the polypropylene/glass fiber system,[2,3,5] the polypropylene/mica system,[6,9] the polypropylene/carbon fiber system,[7] the nylon-66/carbon fiber system,[4] and the poly(ethylene terephthalate)/glass fiber system[8] was reported.

Studies on the distribution of higher-order structures in injection moldings of filled plastics are very few.[13–16] Kamal et al.[13] measured on an injection molding of polypropylene filled with 10 wt % glass fibers the distributions in the thickness direction, of the content and orientation state of glass fibers and the distributions in the flow and thickness directions, of the degrees of crystalline and amorphous orientations by infrared dichroism. As the result, they found that crystalline molecular chains were oriented perpendicular to the flow direction and the degree of the orientation was higher nearer the gate and surface and was increased by the filling of glass fibers. Furthermore, they found that amorphous molecular chains were oriented to the flow direction and the degree of the orientation was higher nearer the gate and surface and was increased by the filling of glass fibers. Bayer et al.[14,15] injection-molded bars from high density polyethylenes filled with carbon black at levels of 0–7.5 vol % by an elongation flow injection molding method, measured the variation of birefringence in the thickness direction, and showed that there existed a maximum of molecular orientation near the surface. The authors[16] studied the crystal orientation state in injection moldings of talc-filled polypropylenes and showed that the plate planes of talc particles were aligned parallel to the surface of injection molding and that the c- and a^*-axes of polypropylene crystals were bimodally oriented to the flow direction and the b-axis, which is the growth direction of polypropylene crystal was oriented to the thickness direction; Although the degree of the bimodal orientation of c- and a^*-axes decreased toward the interior of the injection molding, the b-axis orientation was strong throughout the thickness direction.

In the present paper, we will report studies on the influences of the kind and content of fillers and cylinder temperature on distributions in the flow and thickness directions, of higher-order structures such as crystallinity, β-crystal content, thickness of skin layer, a^*-axis-oriented component fraction, degree of b-axis orientation to the thickness direction, and crystalline orientation functions in injection moldings of talc- or calcium carbonate-filled polypropylenes. In addition, a theoretical analysis of molecular orientation process will be presented.

EXPERIMENTAL

Samples

Polypropylene used was homoisotactic polypropylene powder, Grade PN 120, which was produced by Tokuyama Soda Co., Ltd. and had a melt flow index (MFI) of 2 dg/min.

Fillers used were Crown Talc-Z (hereinafter abbreviated as TC) which was a talc produced by Matsumura Industry Co., Ltd. and had an average diameter of 10 μm and Stavigot 15A (hereinafter abbreviated as CC) which was a precipitated calcium carbonate produced by Shiraishi Industry Co., Ltd. and surface-treated with an aliphatic acid and had an average diameter of 0.2 μm. Figure 1 shows the

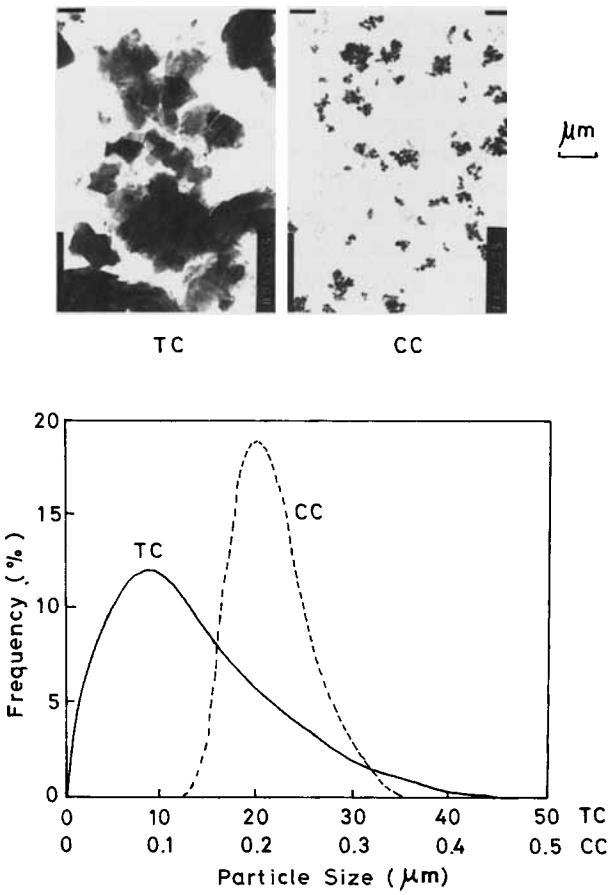

Figure 1 Transmission electron micrographs and particle size distributions of talc (TC) and calcium carbonate (CC).

transmission electron micrographs and particle size distributions of TC and CC. TC is flaky and has a broad particle size distribution and CC is spherical and has a sharp particle size distribution.

The polypropylene powder was mixed with fixed amount of fillers for 5 min in a 100 L Supermixer, extruded by a CCM extruder with a vent at a kneader temperature of 190°C and an extruder temperature of 220°C into strands which were cut into pellets of about 3 mm size by an automatic cutter. Filler contents were 0, 0.5, 10, 20, 30, 40, and 60 wt %. The filler content of 0.5 wt % was for checking the crystallization nucleation effect of the fillers. Hereinafter, the sample with filler content of 0 wt % is called PP, the sample with TC content of 0.5 wt % is called TC-0.5, the sample with TC content of 10 wt % is called TC-10, and so on, the sample with CC content of 0.5 wt % is called CC-0.5, the sample with CC content of 10 wt % is called CC-10, and so on.

Figure 2 shows the dependences of MFI and die swell ratio at MFI measurement on filler content. MFI decreases nearly linearly with increasing CC content and it somewhat increases at TC contents up to 20 wt % and after that decreases rapidly with increasing TC content. The die swell ratio decreases rapidly with increasing TC content and it somewhat increases at CC contents up to 30 wt % and after that decreases rapidly with increasing CC content.

Injection Molding

Flexural test specimens (ASTM D790) were injection-molded using an 8 oz Nikko Ankerwerk V22A-120 type reciprocating-screw injection molding machine. The shape of the test specimen is shown in Figure 3. A polymer reservoir was provided to make resin flow in the specimen uniform. The gate size measured 7.0 mm wide, 1.5 mm thick, and 3.0 mm long. The sprue was a truncated cone with 5.4 mm inlet diameter, 7.4 mm outlet diameter, and 45 mm long and the runner measured 7.0 mm wide, 4.5 mm thick, and 100 mm long. Since cylinder temperature affects the degree of molecular orientation of the product and its mechanical properties more than

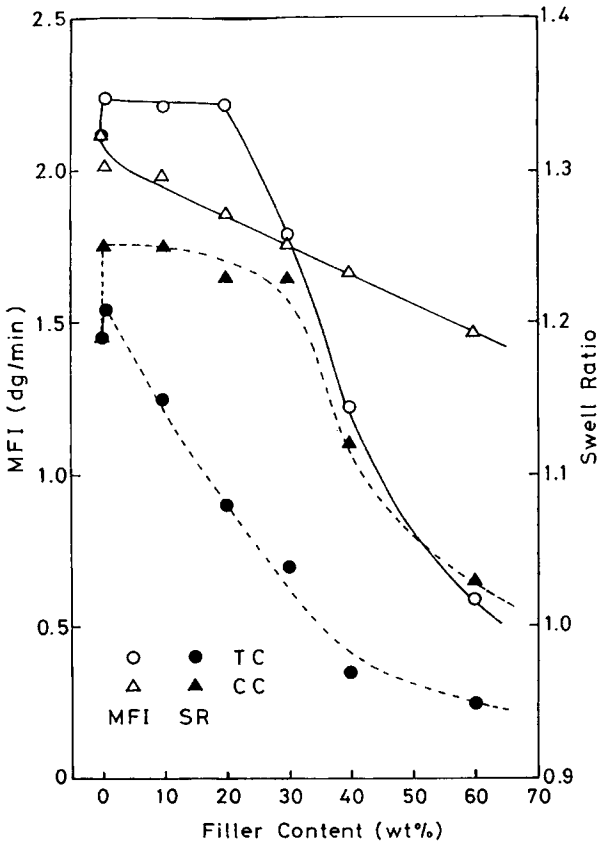

Figure 2 Dependence of MFI and die swell ratio on filler content.

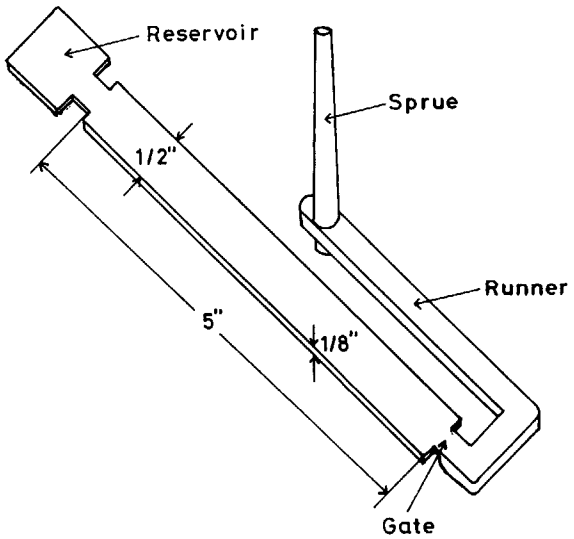

Figure 3 Shape of test specimen.

any other injection molding conditions,[17] injection molding was carried out, varying cylinder temperature only and keeping all other conditions constant. Table I lists injection molding conditions adopted. For cylinder temperature, the temperature of the metering zone (MH3) at the extreme end was used.

Structural Analyses

Mean Higher-Order Structures

An Izod impact test was carried out at 23°C on notched flexural test specimens injection-molded at a cylinder temperature of 240°C. The dispersion states of fillers on the fractured surfaces were observed with a scanning electron microscope, JEOL JSM-T20, under magnifications of 1000 × for TC series and 10,000 × for CC series.

A thin section about 0.1 mm thick was sliced from the central part of the specimen perpendicular to the flow direction (MD) with a microtome and its crystalline texture was observed with a polarizing microscope, Olympus PM-6, under a magnification of 20 ×. The thicknesses of the skin layers of both surfaces were averaged.

A wide-angle X-ray diffraction pattern was taken at the central part of the specimen by setting its MD in accord with the meridian using a Rigaku Denki RU-200 diffractometer with Ni-filtered Cu-K_α radiation at a sample-to-film distance of 45 mm. Using a goniometer, 2θ scan was carried out at a scan speed of 4°/min and azimuthal scans of the (110) and (040) plane reflections were carried out at a scan speed of 8°/min, and crystalline orientation functions f_{a^*}, f_b, and f_c were calculated according to the Wilchinsky's method.[18] a^*-Axis-oriented component fraction $[A^*]$ was obtained by the method described in the Results section. 2θ scan was carried out at the central part of the specimen using a rotating specimen table and the crystallinity X_c was calculated according to Weidinger and Hermans' method.[19]

Owing to the absorption of X-ray by the fillers, good diffractions could be obtained only at TC contents up to 40 wt % and CC contents up to 20 wt %.

Distribution of Higher-Order Structures in Flow Direction

Since the length of the specimen was about 12.7 cm, the thickness of the skin layer, $[A^*]$, and crystalline orientation functions at the parts 2.1, 4.2, 6.3, 8.4, and 10.5 cm far from the gate were measured by the methods described in the previous section.

These measurements were carried out on specimens molded from PP, TC-10, and CC-10 at each cylinder temperature and specimens molded from other samples at a cylinder temperature of 240°C.

Table I Injection Molding Conditions

Expt No.	Cylinder Temperature (°C) MH1[a]	MH2[b]	MH3[c]	DH[d]	Injection Pressure (kg/cm²)	Injection Speed (cc/s)	Mold Temperature (°C)	Cooling Time (s)
1	160	190	200	190	500	13.5	40	40
2	160	220	240	220	500	13.5	40	40
3	160	250	280	250	500	13.5	40	40
4	160	280	320	280	500	13.5	40	40

[a] Feed zone.
[b] Compression zone.
[c] Metering zone.
[d] Die head.

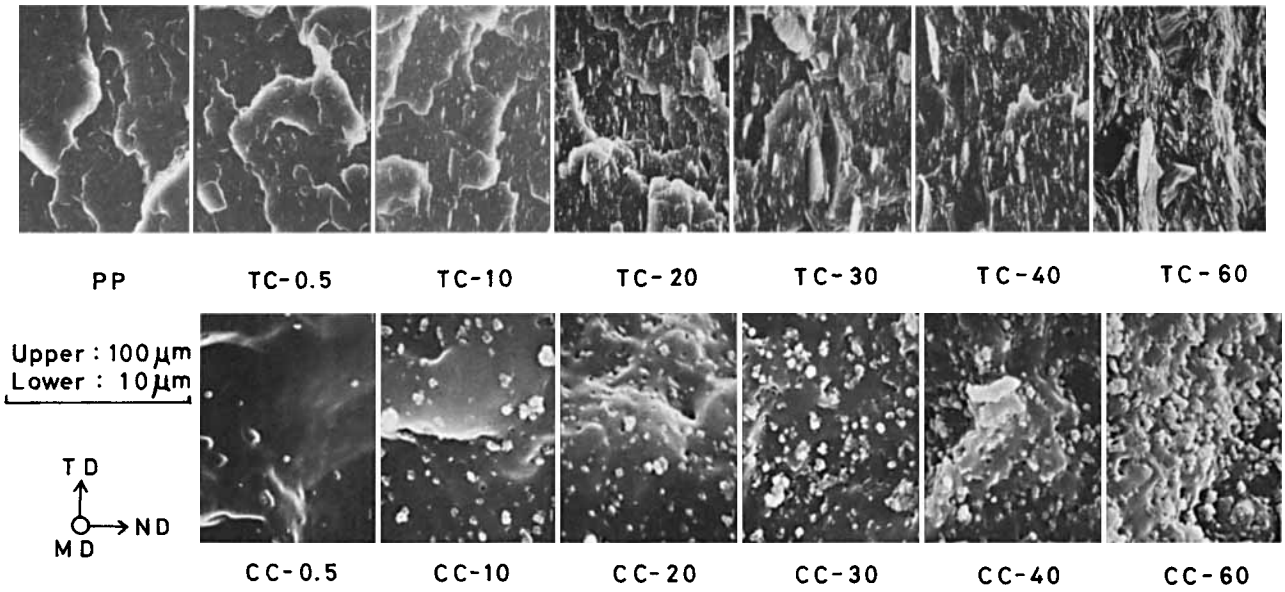

Figure 4 Dispersion states of fillers in injection-molded specimens.

Distribution of Higher-Order Structures in Thickness Direction

X_c, $[A^*]$, and the crystalline orientation functions were measured by the methods described in the previous section on thin sections about 0.3 mm thick slices successively from the surface to the center at the central parts of specimens. Wide-angle X-ray diffractograms were measured on the same sections using the rotating specimen table and the ratios the (040) plane reflection intensities $I(040)$ to the (110) plane reflection intensities $I(110)$, $I(040)/I(110)$, were obtained in order to study the degree of b-axis orientation to the thickness direction[16] and the β-crystal contents, K values, were obtained according to Turner-Jones et al.'s method.[20]

These measurements were carried out on specimens molded from PP, TC-10, and CC-10 at each cylinder temperature and specimens molded from other samples at a cylinder temperature of 240°C. These measurements were possible at TC and CC contents up to 40 wt %.

RESULTS

Mean Higher-Order Structures

Figure 4 shows scanning electron micrographs of fractured surfaces at the parts 0.5 mm far from the surfaces of specimens molded at a cylinder temperature of 240°C. TC particles are aligned parallel to the surface of the specimen and their dispersion is good at each content. CC particles do not completely disperse to the primary particle and somewhat agglomerate, but their dispersion is considerably good.

Figure 5 shows the dependence of mean crystallinity X_c on cylinder temperature. X_c is not so much increased by CC filling and considerably increased by TC filling. This is assumed to be because although CC has almost no crystallization nucleation ability, TC has a notable ability as shown in Figure 25. X_c

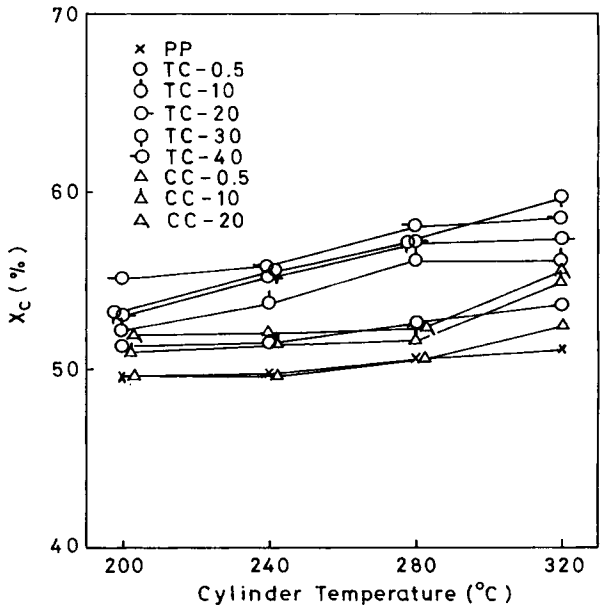

Figure 5 Dependences of crystallinity X_c on cylinder temperature.

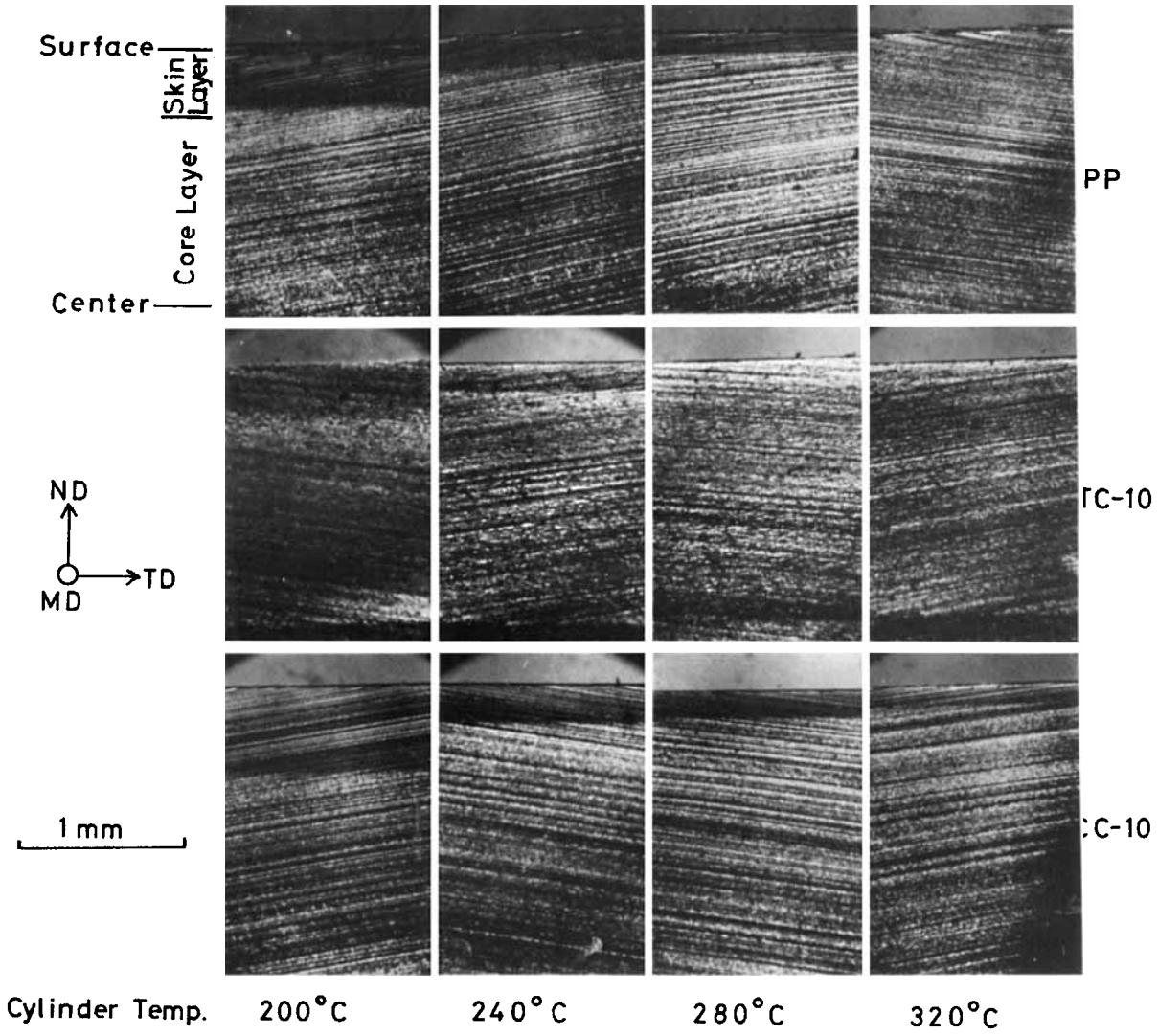

Figure 6 Changes with cylinder temperature, of polarized micrographs of unfilled and filled injection moldings.

tends to increase with increasing cylinder temperature, which is because the higher the cylinder temperature, the higher the injected resin temperature, which takes longer time to be cooled and the cooling rate is low.

Figure 6 exemplifies polarized micrographs of thin sections cut perpendicular to the flow direction (MD) from specimens molded from PP, TC-10, and CC-10 at each cylinder temperature. Clear skin/core structures are observed. The thickness of the skin layer decreases with increasing cylinder temperature and comparison at the same cylinder temperature shows that the skin layers of TC-10 and CC-10 are thicker than that of PP. Observation of all specimens showed that the skin/core structure became more obscure with increasing TC and CC contents as in the results of Xavier et al.[3,9] on glass fiber- or mica-filled polypropylenes and of Morales and White[12] on spiolite- or talc-filled polypropylenes, but the skin layer could be observed at TC and CC contents up to 40 wt %.

Figure 7 shows the dependence of the thickness of the skin layer on cylinder temperature. The thickness of the skin layer decreases with increasing cylinder temperature. In contrary to the results of Xavier et al.[3,9] on glass fiber- or mica-filled polypropylenes and in accord with the results of Morales and White[12] on spiolite- or talc-filled polypropylenes, the thickness of the skin layer increases with increasing TC and CC contents.

Figure 8 exemplifies wide-angle X-ray diffraction patterns of specimens molded from PP, TC-10, and

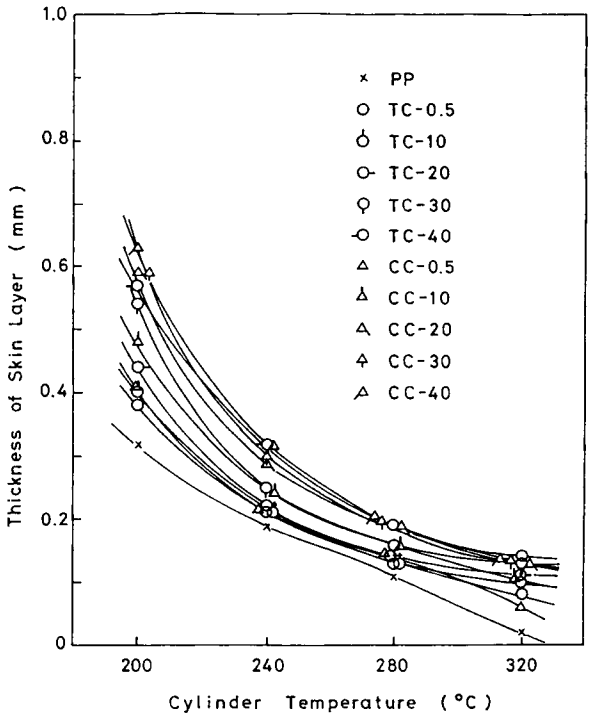

Figure 7 Dependences of thickness of skin layer on cylinder temperature.

CC-10 at a cylinder temperature of 200°C. They show that fiber patterns of the c-axis and a^*-axis mixed orientations overlap on Debye rings.

Figure 9 exemplifies the 2θ scan curve and (110) plane and (040) plane azimuthal scan curves of a specimen molded from TC-10 at a cylinder temperature of 200°C. Here, in order to evaluate the proportions of the c-axis-oriented component and a^*-axis-oriented component, the following procedure is carried out: A base line (BL2) is drawn horizontally at the bottom of the azimuthal scan curve of the (110) reflection; the area around an azimuthal angle of 0° above the base line is taken as C and the area around an azimuthal angle of 90° above the base line is taken as A^*; the c-axis-oriented component fraction $[C]$ and the a^*-axis-oriented component fraction $[A^*]$ are defined as follows:

$$[C] = \frac{C}{C + A^*} \tag{1}$$

$$[A^*] = \frac{A^*}{C + A^*} \tag{2}$$

Although there is no assurance that the absolute amounts of c-axis-oriented and a^*-axis-oriented components can be rigorously evaluated by $[C]$ and $[A^*]$, a relative comparison may be made by them when raw resin and/or molding conditions are changed. Also, the crystalline orientation functions (a^*-axis orientation function f_{a^*}, b-axis orientation function f_b, and c-axis orientation function f_c) were calculated from the (110) plane and (040) plane

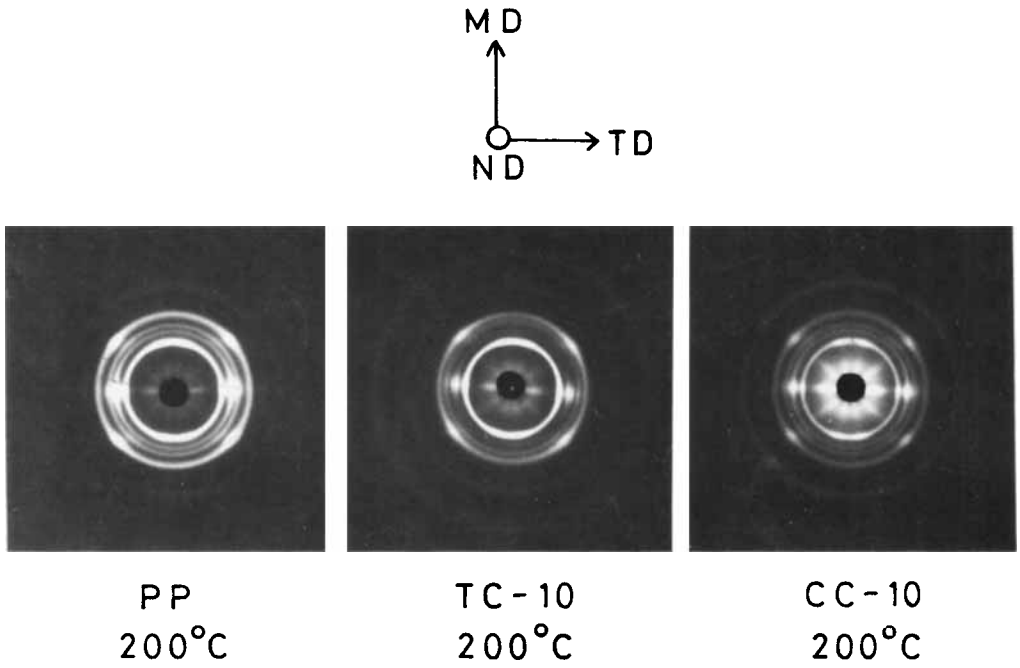

Figure 8 Wide-angle X-ray diffraction patterns of specimens molded from PP, TC-10, and CC-10 at cylinder temperature of 200°C.

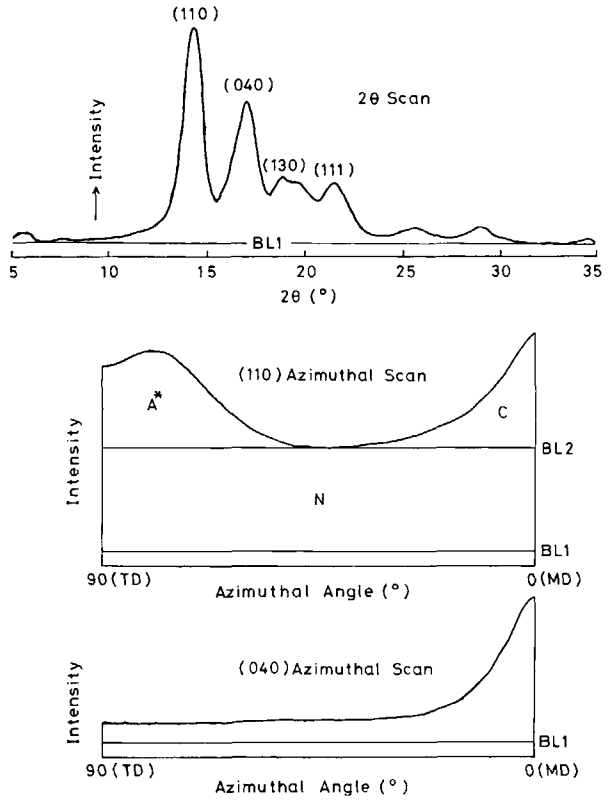

Figure 9 2θ scan curve and (110) and (040) plane azimuthal scan curves of specimen molded from TC-10 at cylinder temperature of 200°C.

azimuthal scan curves according to Wilchinsky's method.[18]

Figure 10 shows the dependence of the a^*-axis-oriented component fraction $[A^*]$ on cylinder temperature. CC series show similar behaviors to that of PP and their $[A^*]$'s increase with increasing cylinder temperature. Namely, it means that the fraction of the a^*-axis-oriented component as against to that of the c-axis-oriented component increases with increasing cylinder temperature in PP and CC series. On the other hand, $[A^*]$'s of TC series scarcely depend on cylinder temperature and are lower than that of PP. Namely, the filling of TC decreases the a^*-axis-oriented component and increases the c-axis-oriented component.

Figure 11 exemplifies the dependences of the orientation functions of the specimens molded from PP, TC-10, and CC-10 on cylinder temperature. The

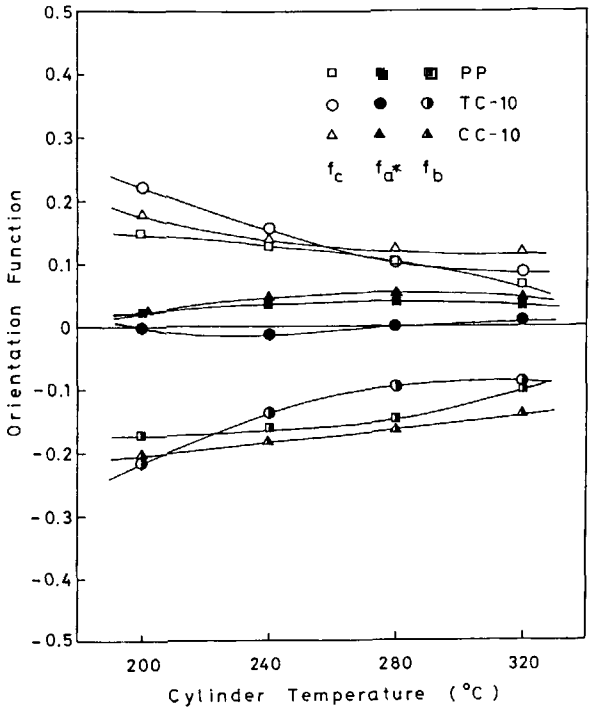

Figure 11 Dependences of crystalline orientation functions on cylinder temperature.

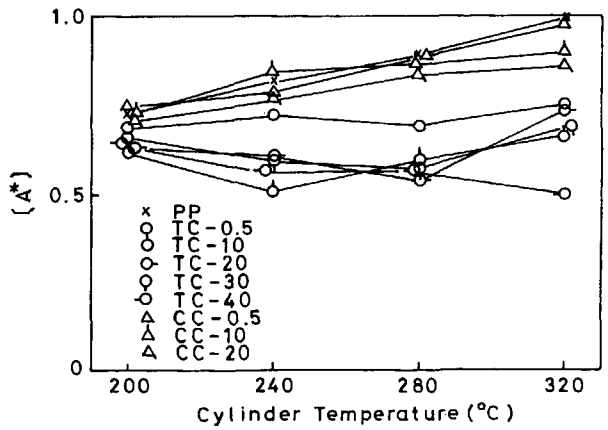

Figure 10 Dependences of a^*-axis-oriented component fraction $[A^*]$ on cylinder temperature.

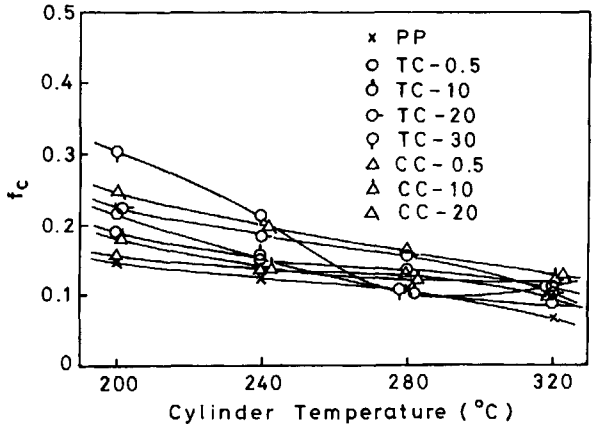

Figure 12 Dependences of c-axis orientation function f_c on cylinder temperature.

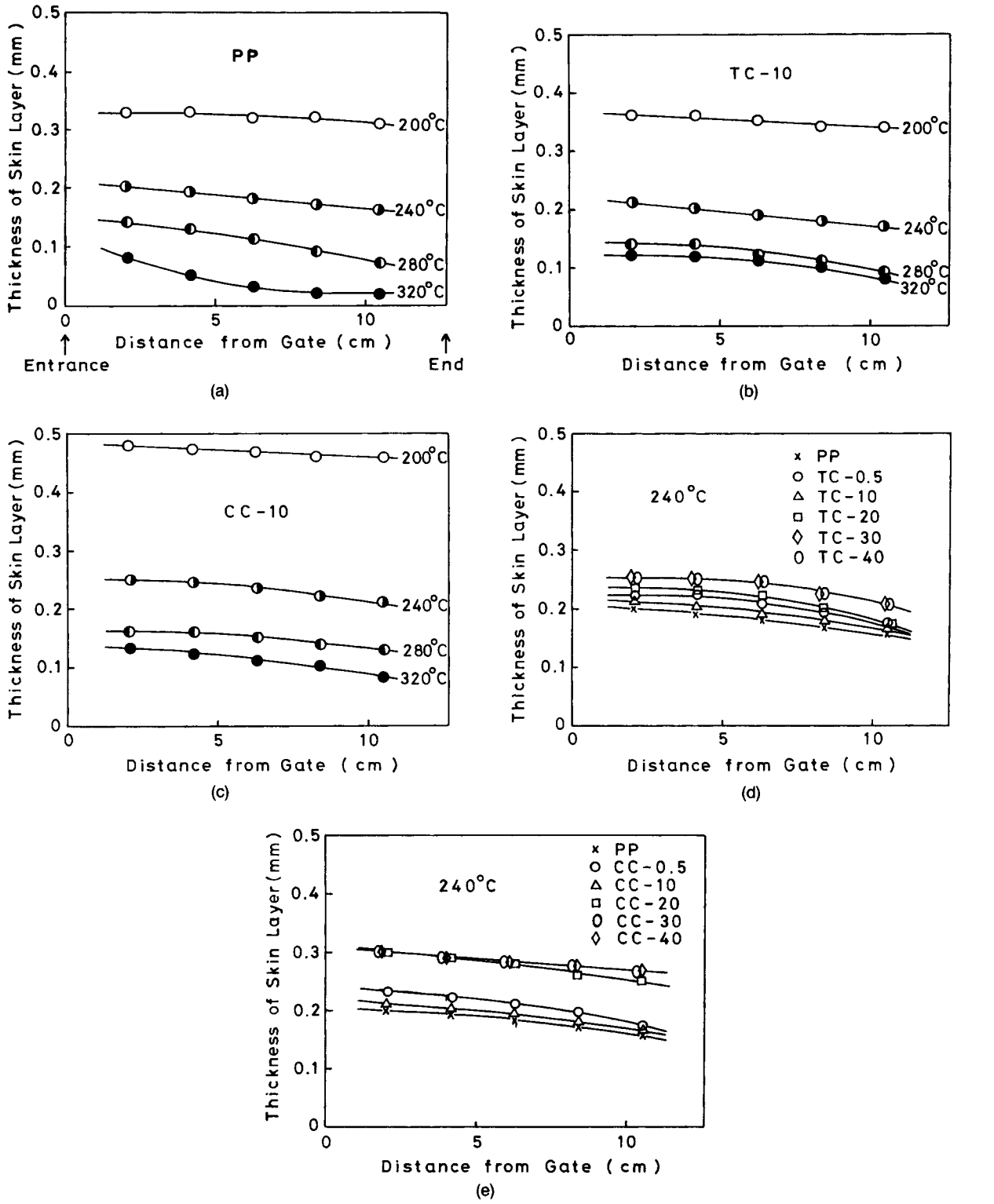

Figure 13 Distribution of thickness of skin layer in flow direction. (a) PP molded at various cylinder temperatures. (b) TC-10 molded at various cylinder tempertures. (c) CC-10 molded at various temperatures. (d) TC series molded at 240°C. (e) CC series molded at 240°C.

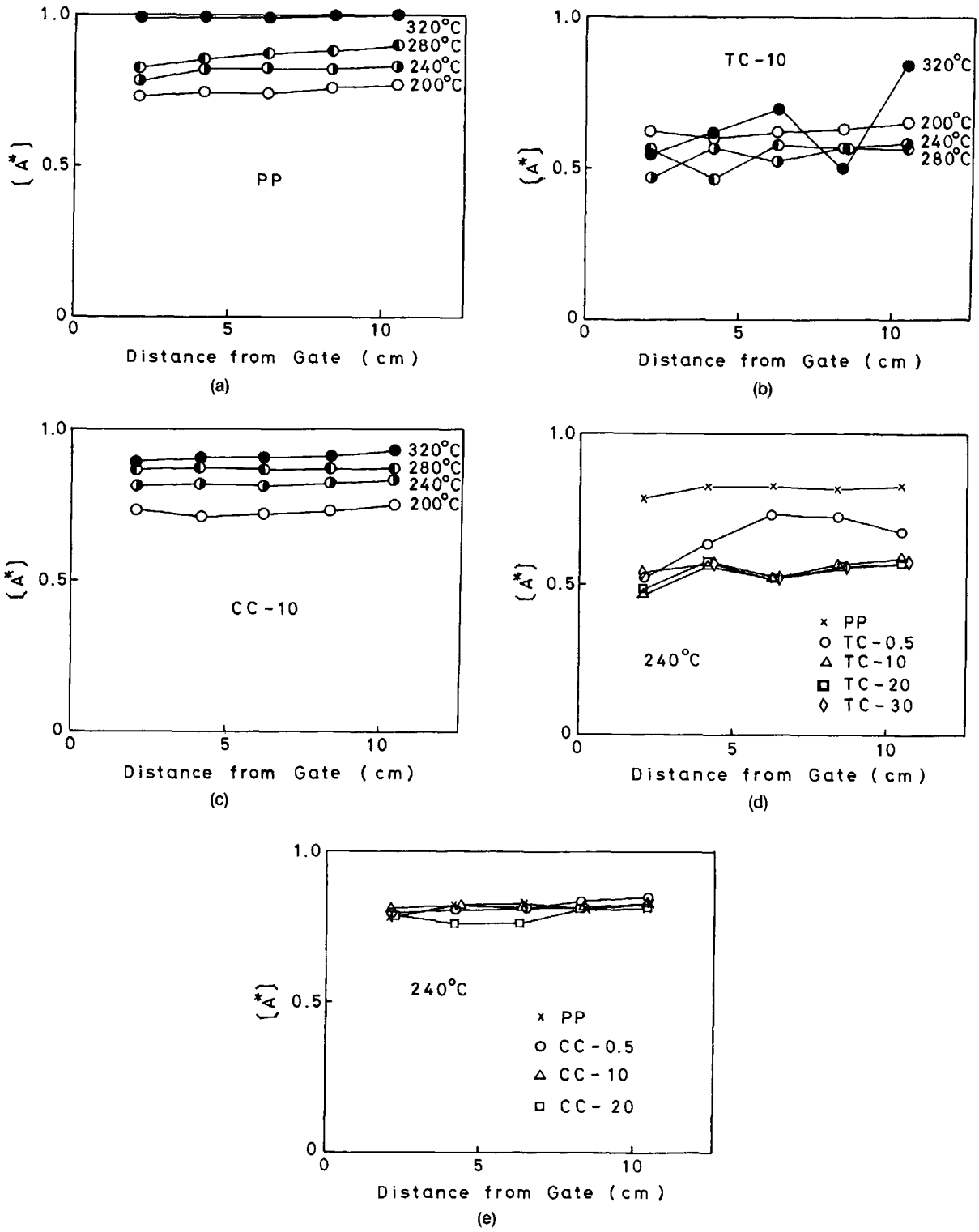

Figure 14 Distribution of a^*-axis-oriented component fraction $[A^*]$ in flow direction. (a) PP molded at various cylinder temperatures. (b) TC-10 molded at various cylinder temperatures. (c) CC-10 molded at various cylinder temperatures. (d) TC series molded at 240°C. (e) CC series molded at 240°C.

absolute values of the c-axis orientation function f_c and b-axis orientation function f_b decrease with increasing cylinder temperature and the a^*-axis orientation function f_{a^*} somewhat increases with increasing cylinder temperature for PP. Generally, TC and CC series show similar tendencies to that of PP except for f_{a^*}'s of TC series, which scarcely depend on cylinder temperature and are nearly 0.

Figure 12 shows the dependence of the c-axis orientation function f_c on cylinder temperature. f_c decreases with increasing cylinder temperature and comparison at the same cylinder temperature shows that it increases with increasing filler content.

β-crystal content could not be evaluated since the reflection intensity of wide-angle X-ray diffraction of β-crystals was weak.

Distribution of Higher-Order Structures in Flow Direction

Figures 13(a)-(e) show the distributions of the thickness of the skin layer in the flow direction. The thickness of the skin layer increases with decreasing cylinder temperature and with increasing filler content and decreases with going away from the gate. The decreasing rate of the thickness of the skin layer in the flow direction increases with going away from the gate, with increasing cylinder temperature, and with decreasing filler content, except for the specimen molded from PP at a cylinder temperature of 320°C. Altendorfer and Seitl[21] and Krsova[22] observed similar tendencies in injection-molded polypropylenes. Hirose et al.,[23] Altendorfer et al.,[24,25] Koppelmann et al.,[26,27] and Menges et al.[28] reported that the thickness of the skin layer showed a maximum near the gate in injection-molded polypropylenes. Although no maximum is observed near the gate in the present experiment as in the case of injection-molded polypropylenes in the previous paper,[29] there is almost no decrease in the thickness of the skin layer near the gate.

Figures 14(a)-(e) show the distribution of the a^*-axis-oriented component fraction $[A^*]$ in the flow direction. $[A^*]$'s of PP and CC series increase with increasing cylinder temperature and increase a little with going away from the gate. There is almost no influence of CC filling. $[A^*]$'s of TC series scarcely depend on cylinder temperature and increase a little with going away from the gate. TC filling decreases $[A^*]$.

Figure 15 exemplifies the distributions in the flow direction of the orientation functions of specimens molded from PP, TC-10, and CC-10 at a cylinder temperature of 240°C. The absolute values of f_c and f_b decrease with going away from the gate and f_{a^*} is nearly constant for PP. Generally, TC and CC series show similar tendencies to that of PP except for f_{a^*}'s of TC series which have low values and show minima at midway parts in the flow direction.

Figures 16(a)-(e) show the distributions of the c-axis orientation function f_c in the flow direction. f_c is higher as cylinder temperature is lower and TC content is higher, and decreases with going away from the gate. f_c is scarcely influenced by CC filling of up to 20 wt %. Trotignon et al.[30-32] found that the crystalline orientation A, which was obtained from the (110) and (111) plane reflection intensities in X-ray diffraction and the crystalline and amorphous orientations, f_{cr} and f_{am}, measured by infrared dichroism in injection-molded polypropylenes decreased with going away from the gate. Murphy et al.[33,34] also obtained similar results on A. Altendorfer and Seitl[21] and Menges et al.[28,35] obtained similar results on the orientation degree measured by birefringence. Kubota[36] reported that the orientation degree measured by fluorescence showed a maximum at a midway part in the flow direction of a rectan-

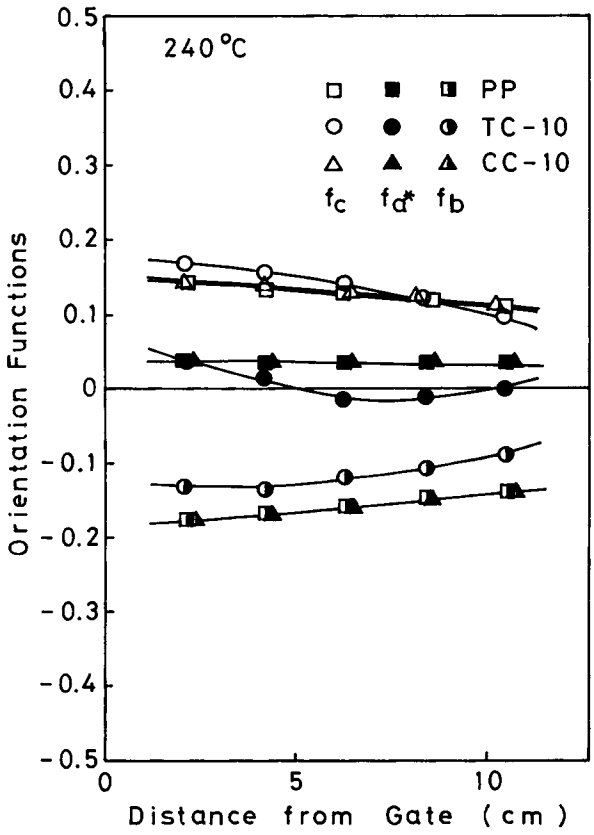

Figure 15 Distributions of crystalline orientation functions in flow direction. PP, TC-10, and CC-10 molded at cylinder temperature of 240°C.

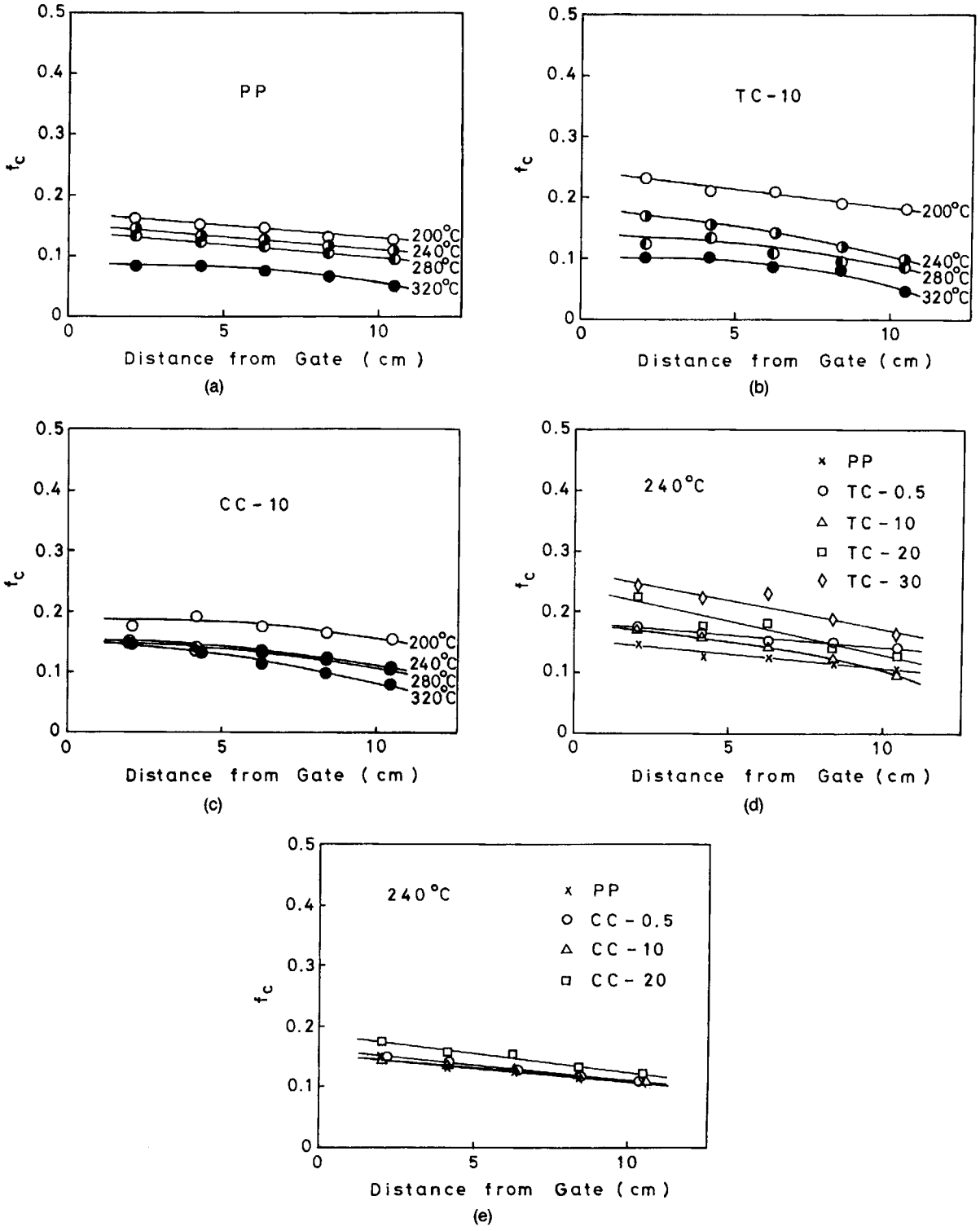

Figure 16 Distribution of c-axis orientation function f_c in flow direction. (a) PP molded at various cylinder temperatures. (b) TC-10 molded at various cylinder temperatures. (c) CC-10 molded at various cylinder temperatures. (d) TC series molded at 240°C. (e) CC series molded at 240°C.

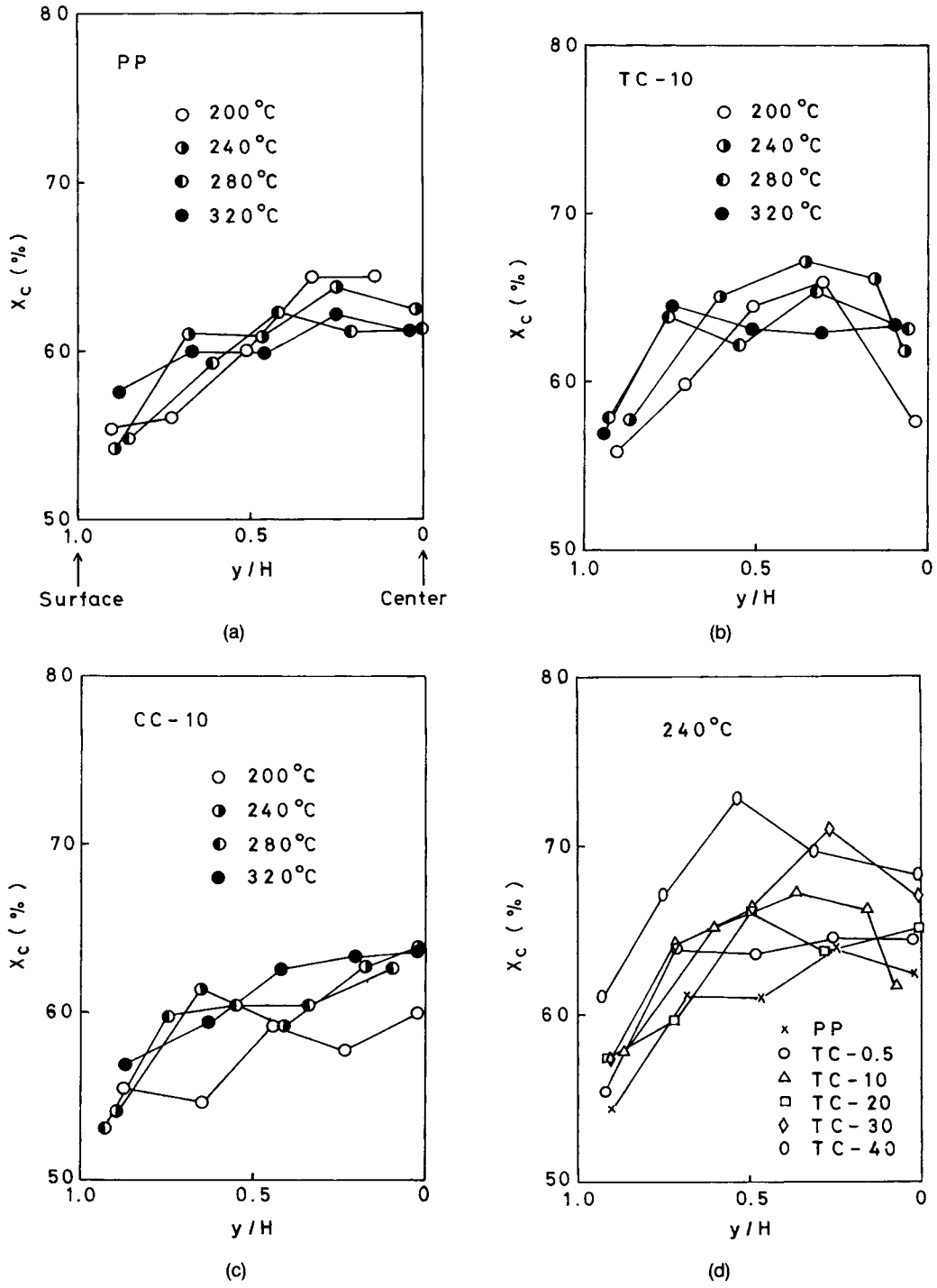

Figure 17 Distribution of crystallinity X_c in thickness direction. (a) PP molded at various cylinder temperatures. (b) TC-10 molded at various cylinder temperatures. (c) CC-10 molded at various cylinder temperatures. (d) TC series molded at 240°C. (e) CC series molded at 240°C.

gular plate. Kamal et al.[13] measured, by infrared dichroism, the degrees of crystalline and amorphous orientations of an injection molding of polypropylene filled with 10 wt % glass fibers and found that both orientations increased by glass fiber filling and decreased with going away from the gate, agreeing with the present results.

Since the reflection intensity by the β-crystals was weak, the distribution of β-crystal content in the flow direction could not be evaluated.

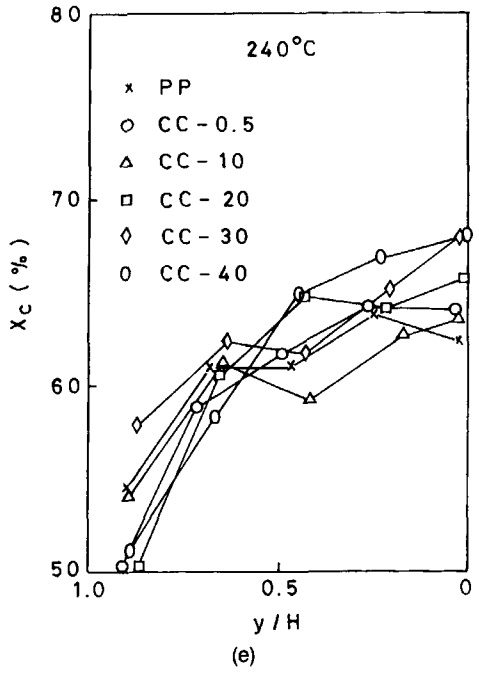

Figure 17 (*Continued from previous page*)

Distribution of Higher-Order Structures in Thickness Direction

Figures 17(a)–(e) show the distributions of crystallinity X_c in the thickness direction. Here, H is half of the thickness of specimen and y is the distance from the center. X_c is low at the surface region and increases toward the interior. This is because the inner region is cooled more slowly. It seems that cylinder temperature scarcely influences X_c. CC filling scarcely influences X_c and TC filling increases X_c. Houska and Brummell[37,38] showed that X_c's of an injection-molded polypropylene measured by infrared spectrum and density showed minima at the surface skin region and increased toward the interior. Trotignon and Verdu[31,32] obtained X_c's of injection-molded polypropylenes from the heat of fusion measured by differential scanning calorimetry, which showed, contrary to Houska et al.'s results, maxima at the skin region, decreased once, and increased toward the interior. Since our, Houska et al.'s, and Trotignon et al.'s results differ in the measuring method of X_c, they cannot be absolutely compared, particularly at the surface region of specimen where the degree of molecular orientation is high. However, they agree in the point that X_c increases toward the interior in the inner region, where the degree of molecular orientation is low.

Figures 18(a)–(e) show the distributions of β-crystal content, K value, in the thickness direction. Except for the surface regions of the specimen molded from CC-10 at a cylinder temperature of 200°C, the K value is higher nearer the surface and decreases toward the interior. The K value is generally higher as cylinder temperature is lower. Although TC filling decreases K value, CC filling increases it. The reason for this is not obvious at the present time. The skin regions are shown in Figures 18(a)–(c), which show that the K value is high at the region of about twice the thickness of the skin layer and that β-crystals exist at the surface region of about twice the thickness of the skin layer. As can be seen from the case of the specimen molded from CC-10 at a cylinder temperature of 200°C, it seems that β-crystals do not exist so much at the surface skin region but exist most at the region inside the skin layer. Kantz et al.[39] found that the β-crystals existed in the shear zones inside the skin layer of injection-molded polypropylene. Fitchmun and Mencik[40] found from polarizing microscopy that the β-crystals existed at the boundary between the oriented layer (layer 3) and the core layer. Trotignon and Verdu[31] also found that the β-crystal content was maximum at the region inside the skin layer. Since β-crystals reduce the impact strength of injection-molded polypropylene,[33,34] it is desirable to suppress their formation to the utmost.

Figures 19(a)–(e) show the distributions in the thickness direction, of the wide-angle X-ray diffraction intensity ratio $I(040)/I(110)$, which express the degree of b-axis orientation to the thickness direction.[16] The lower the value of $I(040)/I(110)$, the higher the degree of b-axis orientation to the thickness direction. PP and CC series show similar tendencies where the intensity ratio is somewhat high near the surface, decreases once, and increases toward the interior. CC filling scarcely influences the intensity ratio. TC series show very low intensity ratios and long minimum regions. TC filling of a very small amount of 0.5 wt % markedly decreases the intensity ratio and a larger amount of filling has no more effect. The orientation state of polypropylene crystals in injection molding of talc-filled polypropylene has been studied in detail in our previous paper.[16]

Figures 20(a)–(e) show the distributions of the a^*-axis-oriented component fraction $[A^*]$ in the thickness direction. In these figures, since the degree of molecular orientation is very low around the central region, there is some problem in evaluating $[A^*]$ and the precision of $[A^*]$ is not good around the central region. PP and CC series show similar tendencies where $[A^*]$ is high and nearly equal to unity at midway regions of $0.2 \lesssim y/H \lesssim 0.6$ in the thickness direction, which means that there is little c-

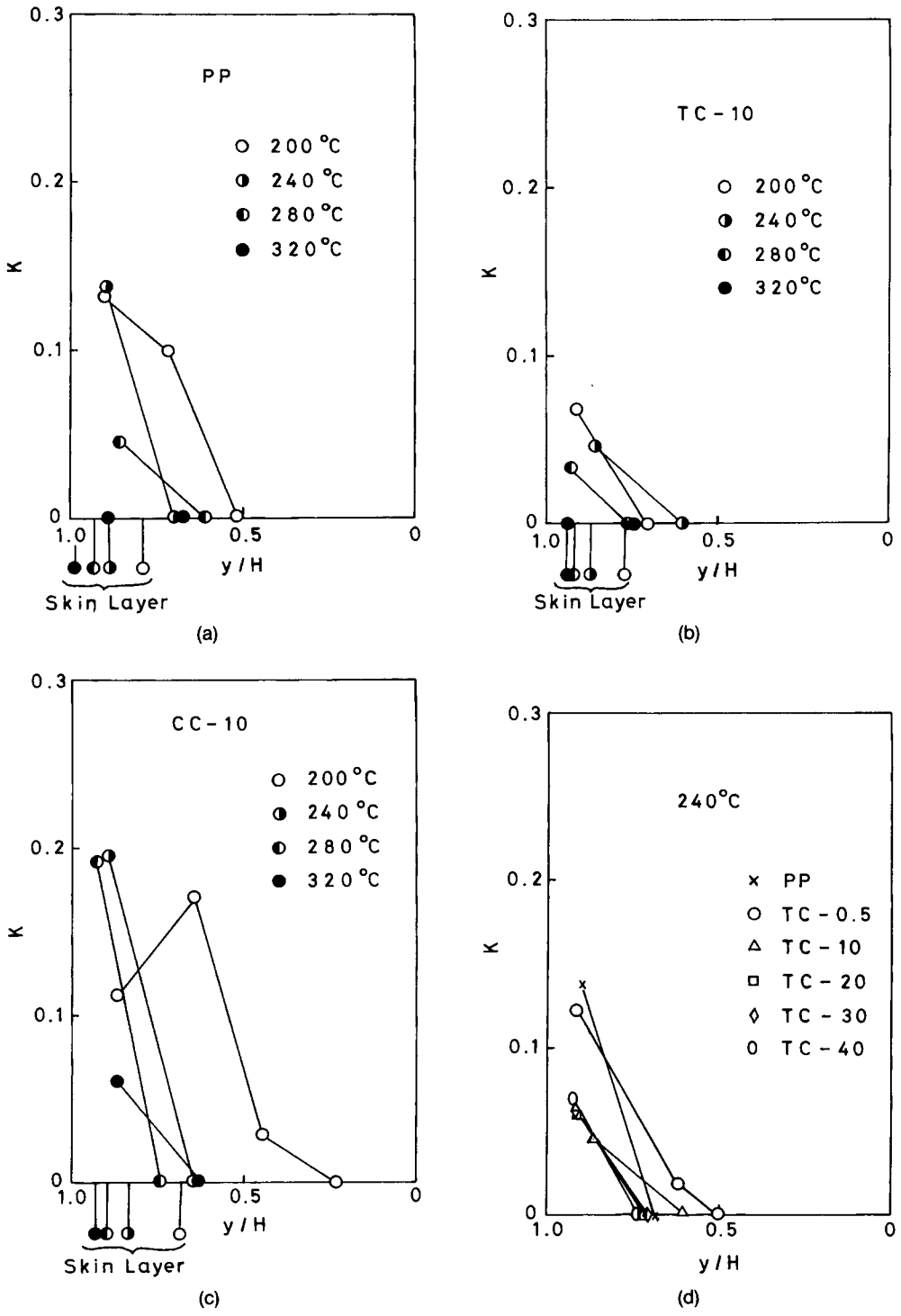

Figure 18 Distribution of β-crystal content, K value, in thickness direction. (a) PP molded at various cylinder temperatures. (b) TC-10 molded at various cylinder temperatures. (c) CC-10 molded at various cylinder temperatures. (d) TC series molded at 240°C. (e) CC series molded at 240°C.

axis-oriented component and most crystals show the a^*-axis orientation at $0.2 \lesssim y/H \lesssim 0.6$, and $[A^*]$ at surface regions is higher as cylinder temperature is higher. CC filling scarcely influences $[A^*]$. TC filling decreases $[A^*]$ and $[A^*]$ tends to decrease toward the interior in TC series. It may be said that the fraction of the a^*-axis-oriented component as against to that of the c-axis-oriented component de-

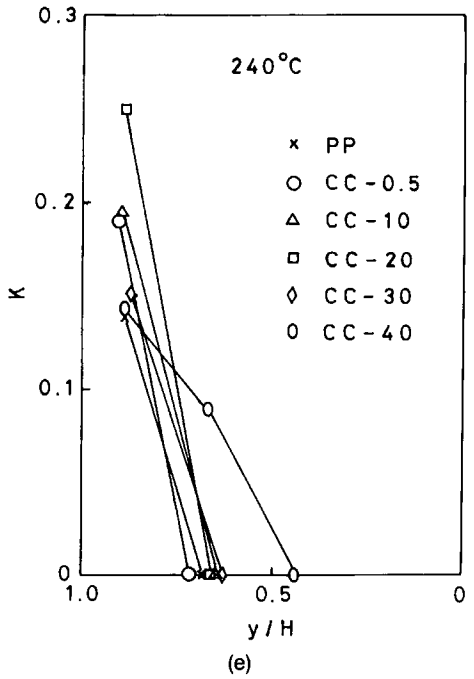

Figure 18 *(Continued from previous page)*

creases across almost all regions in the thickness direction by TC filling.

Figure 21 exemplifies the distributions in the thickness direction, of crystalline orientation functions of specimens molded from PP, TC-10, and CC-10 at a cylinder temperature of 240°C. The absolute values of f_c's and f_b's are higher nearer the surface and f_{a^*}'s show maxima at midway regions. PP and CC-10 show considerably high values of f_{a^*} and TC-10 shows lower values of f_{a^*}. Similar results were obtained for the specimens molded from other samples at other cylinder temperatures. The distributions of crystalline orientation functions have been studied on injection-molded high density polyethylenes by Kamal and Moy.[41-43]

Figures 22(a)–(e) show the distributions of the c-axis orientation function f_c in the thickness direction. f_c is higher nearer the surface and is higher as cylinder temperature is lower at around the surface region. TC or CC filling does not so much influence f_c. There are cases where peaks or shoulders are observed at midway regions in the thickness direction at high cylinder temperatures, which are assumed to be caused by the secondary flow during the cooling and pressure holding process. Koppelmann et al.[26,27,44] measured the distributions in the thickness direction, of birefringences of injection-molded polypropylenes, and found that birefringences at the inner regions of specimens molded with holding pressures were higher than that molded without holding pressure. Hirose et al.,[23] Koppelmann et al.,[26,27,44] and Menges et al.[28] measured the distribution of birefringence in the thickness direction, Trotignon and Verdu[31,32] measured the distribution in the thickness direction, of orientation degree A by X-ray diffraction, and Trotignon and Verdu[31] and Houska and Brummell[37,38] measured the distributions in the thickness direction, of crystalline and amorphous orientation functions f_{cr} and f_{am} by infrared dichroism. They all observed a maximum of molecular orientation at around the surface region. In the present experiment, however, as a possible reason, due to a large slicing interval, no such maximum was observed and f_c decreased gradually from the surface to the interior, except for the cases where the secondary peaks or shoulders caused by the secondary flow appeared. Kubota[36] measured the distribution of the degree of fluorescent orientation in the thickness direction and found that no orientation maximum was observed around the surface region and the degree of orientation decreased gradually from the surface to the interior as in the present results. Kamal et al.[13] measured on an injection molding of polypropylene filled with 10 wt % glass fibers the distributions in the thickness direction, of the degrees of crystalline and amorphous orientations by infrared dichroism, and found that both orientations were higher nearer the surface as in the results of the present experiment.

DISCUSSION

As mentioned above, the influences of the kind and content of filler and cylinder temperature on the distributions of higher-order structures such as crystallinity X_c, β-crystal content K, the degree of b-axis orientation to the thickness direction, $I(040)/I(110)$, a^*-axis-oriented component fraction $[A^*]$, the thickness of skin layer, and crystalline c-axis orientation function f_c in injection moldings of particulate-filled polypropylenes were studied. Those out of these higher-order structures which most influence the product properties, such as mechanical and thermal properties, are the degrees of molecular orientation such as the thickness of the skin layer and f_c. Therefore, we will next theoretically consider the molecular orientation in injection molding.

Many studies have so far been carried out on the molecular orientation process in plastics injection molding.[10,11,17,45-64] The authors regarded recoverable shear strain as a measure of molecular orientation in melt and analyzed the molecular orientation process in injection moldings of polypropylenes and

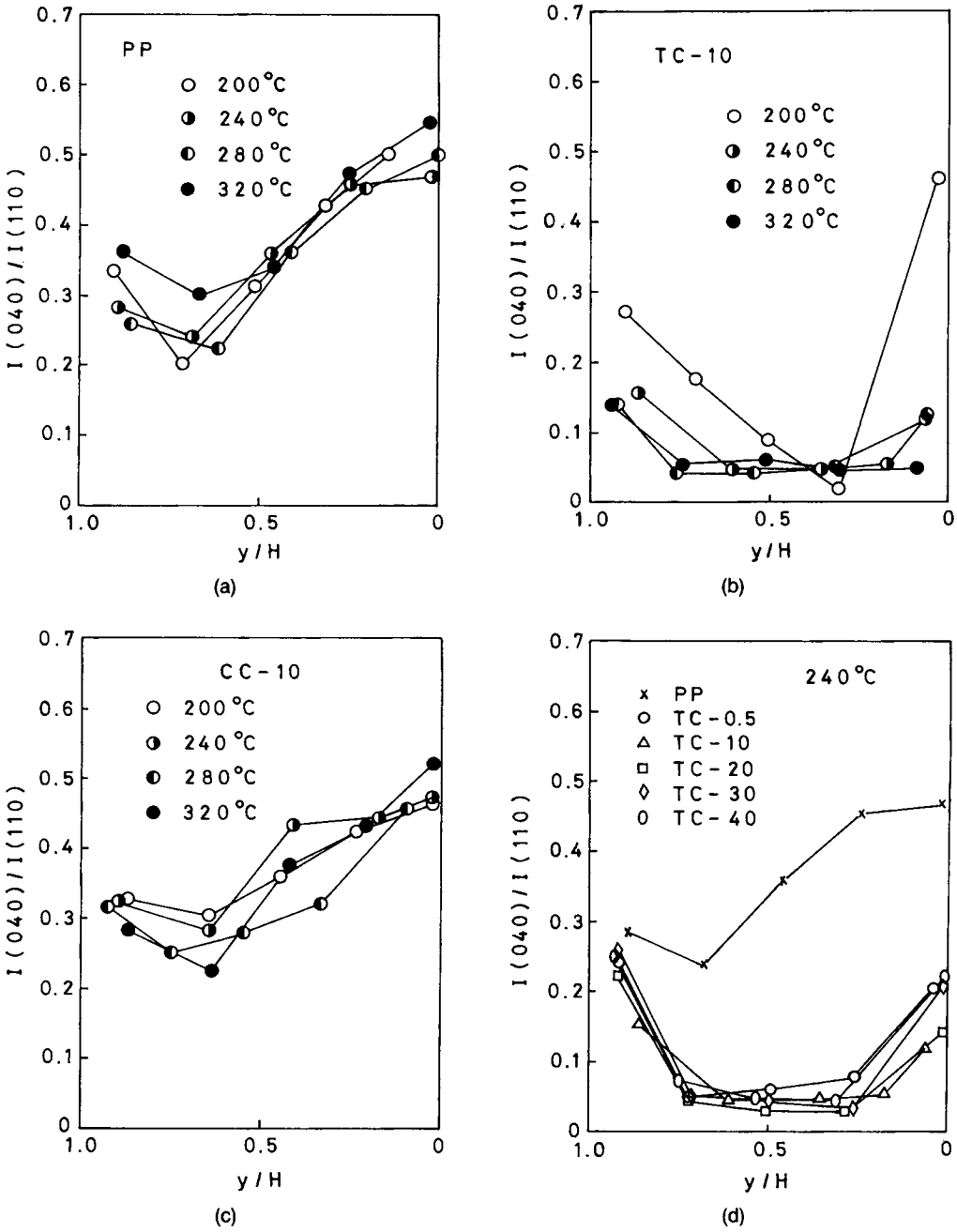

Figure 19 Distribution of wide-angle X-ray diffraction intensity ratio $I(040)/I(110)$ in thickness direction. (a) PP molded at various cylinder temperatures. (b) TC-10 molded at various cylinder temperatures. (c) CC-10 molded at various cylinder temperatures. (d) TC series molded at 240°C. (e) CC series molded at 240°C.

particulate-filled polypropylenes from a viewpoint of growth of a recoverable shear strain at the gate and its relaxation in the cavity.[10,11,17,51,60] Since the variations of molecular orientation in the flow and thickness directions were not studied in detail in our previous papers and the theory was, after that, revised on the value of recoverable shear strain and the treatment of relaxation time of recoverable shear strain, the revised theory and experimental results will be described again.

Theory

In injection molding, a molten resin passes through the sprue, runner, and gate, fills the cavity and becomes a shaped article through cooling and solidi-

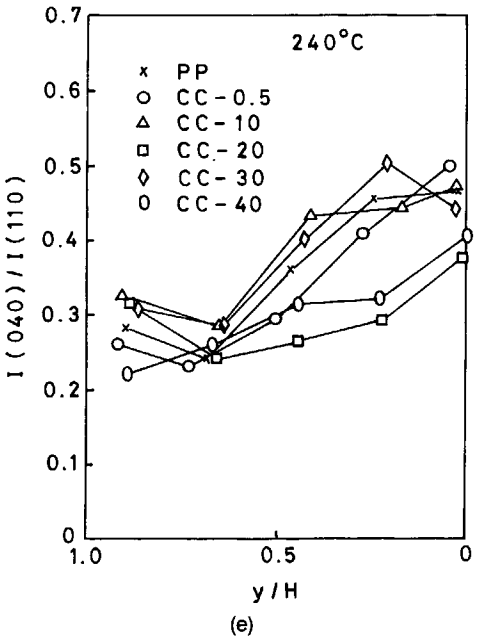

Figure 19 *(Continued from previous page)*

fication. In the meantime, the extent of melt orientation changes at the different parts. As shown in the Experimental section, the cross section of the flow path at the gate is extremely small, compared with the sprue, runner, and cavity and the flow rate is constant throughout the flow path. Therefore, the shear rate at the gate is extremely high and most of the melt orientation takes place during passage through the gate.

In this analysis, recoverable shear strain γ_e is used as a measure of the melt orientation. As shown in Figure 23, the recoverable shear strain having grown during passage through the gate, γ_{e0}, undergoes a Maxwell-type relaxation with a relaxation time λ_1 while flowing through the cavity and becomes γ_{e1}. At this time, cooling is ignored until the resin completely fills the cavity, and the resin temperature is regarded as identical to the injected resin temperature T_{melt}. Therefore, it is regarded that, meanwhile, a relaxation occurs with the relaxation time $\lambda_1(T_{melt})$ at the injected resin temperature T_{melt}. Then, the resin at a certain position x_1 from the gate is cooled by the mold at the temperature T_{mold} and its temperature becomes $T(t)$. The recoverable shear strain γ_{e1} undergoes a temperature-dependent Maxwell-type relaxation with a relaxation time $\lambda_2(T(t))$ and becomes a residual recoverable shear strain γ_{er} when the resin temperature reaches the crystallization temperature T_c. γ_{er} is assumed to be proportional to the degree of orientation of an injection-molded article.

With V for the injection rate, B for the width of the cavity, and $2H$ for the thickness of the cavity, time t_1 taken by the flow to reach the position x_1 from the inlet of the cavity is expressed by

$$t_1 = \frac{2BHx_1}{V} \tag{3}$$

Then, γ_{e1} is calculated by

$$\gamma_{e1} = \gamma_{e0} \exp\left[\frac{-t_1}{\lambda_1(T_{melt})}\right] = \gamma_{e0} \exp\left[\frac{-2BHx_1}{V\lambda_1(T_{melt})}\right] \tag{4}$$

Here, the Carslaw–Jaeger equation for one-dimensional non-steady-state thermal conduction of infinite solid[65] is applied, ignoring the latent heat of crystallization. Then, the time change of the resin temperature $T(t)$ at y $(0 \le y \le H)$ from the center in the thickness direction is expressed by

$$\frac{T - T_{mold}}{T_{melt} - T_{mold}} = 2\sum_{n=0}^{\infty} \frac{(-1)^n}{\pi(n+\frac{1}{2})} \cos\left[(n+\tfrac{1}{2})\frac{\pi y}{H}\right] \times \exp\left[-(n+\tfrac{1}{2})^2\pi^2\frac{\alpha t}{H^2}\right] \tag{5}$$

where α is the thermal diffusivity.

If eq. (5) is rewritten in the form of $t = f(T)$, the residual recoverable shear strain γ_{er} is calculated by

$$\ln\frac{\gamma_{er}}{\gamma_{e1}} = -\int_{T_{melt}}^{T_c} \frac{1}{\lambda_2(T)}\frac{df(T)}{dT}\,dT \tag{6}$$

Half of the cavity thickness, H, is divided into 10 equal parts, the residual recoverable shear strain at the center of each division, $\gamma_{er,i}$, is calculated by eq. (6), and the mean residual recoverable shear strain γ_{er} is calculated by

$$\gamma_{er} = \frac{1}{10}\sum_{i=1}^{10}\gamma_{er,i} \tag{7}$$

The material characteristics needed to calculate γ_{er} are the initial recoverable shear strain γ_{e0}, its relaxation times λ_1, λ_2, the thermal diffusivity α, and the crystallization temperature T_c.

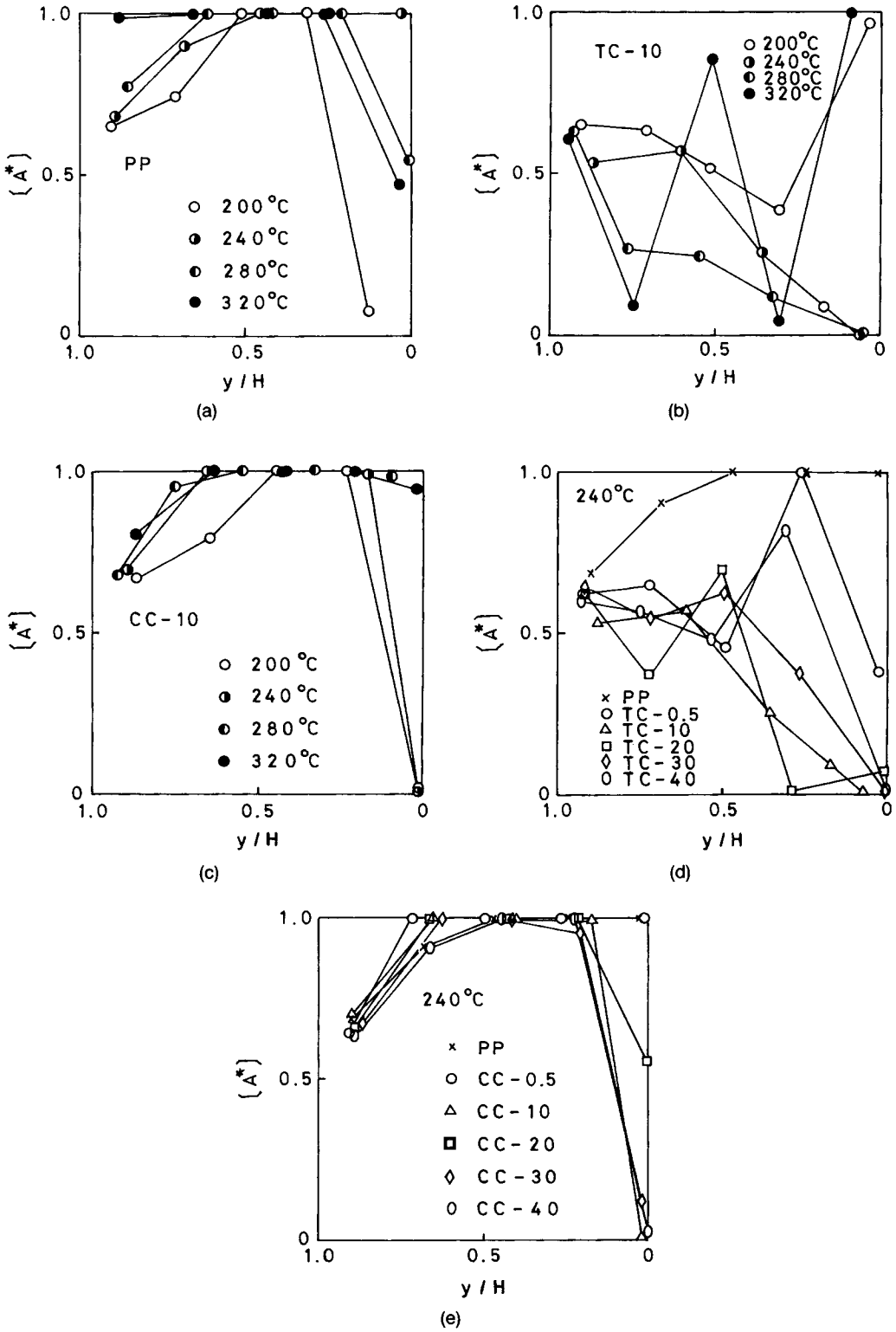

Figure 20 Distribution of a^*-axis-oriented component fraction $[A^*]$ in thickness direction. (a) PP molded at various cylinder temperatures. (b) TC-10 molded at various cylinder temperatures. (c) CC-10 molded at various cylinder temperatures. (d) TC series molded at 240°C. (e) CC series molded at 240°C.

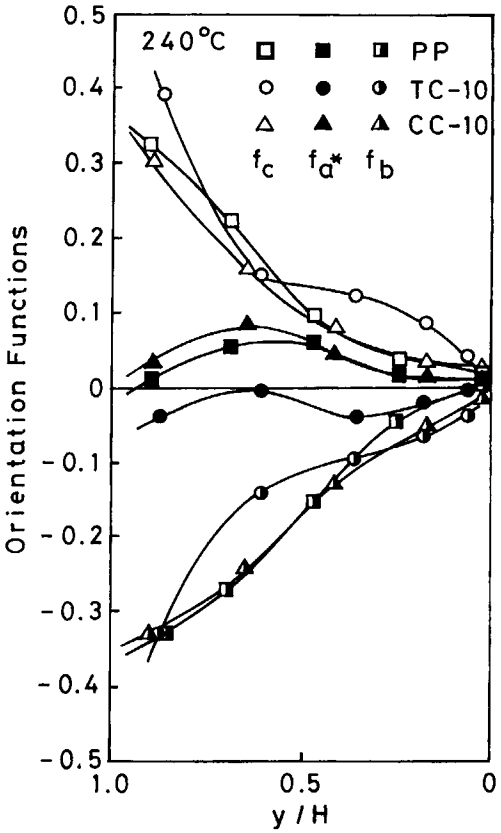

Figure 21 Distributions of crystalline orientation functions in thickness direction. PP, TC-10, and CC-10 molded at cylinder temperature of 240°C.

Experimental

Measurements of Rheological Properties

Recoverable Shear Strain. The recoverable shear strain γ_e was obtained by measuring capillary flow property. According to Heron et al.,[66] the recoverable shear strain in die flow consists of two components: One is the entrance component γ_e(entrance) which grows at the die inlet and the other is the transient component γ_e(transient) which grows in the die land. γ_e(transient) is expressed by[66]

$$\gamma_e(\text{transient}) \simeq \dot{\gamma}_c \lambda(\dot{\gamma}_c)\{1 - \exp[-t_c/\lambda(\dot{\gamma}_c)]\} \quad (8)$$

where $\dot{\gamma}_c$ is the shear rate in the die, $\lambda(\dot{\gamma}_c)$ is the relaxation time at the shear rate of $\dot{\gamma}_c$, and t_c is the residence time in the die. $\lambda(\dot{\gamma}_c)$ is expressed by

$$\lambda(\dot{\gamma}_c) \simeq \lambda_0 \frac{\eta(\dot{\gamma}_c)}{\eta_0} \quad (9)$$

where λ_0 is the relaxation time at the shear rate of 0, $\eta(\dot{\gamma}_c)$ is the shear viscosity at the shear rate of $\dot{\gamma}_c$, and η_0 is the zero-shear viscosity.

γ_e(entrance) was obtained from the end correction coefficient in capillary flow. The relation between pressure P and volumetric flow rate Q was measured with a Koka flow tester manufactured by Shimazu Seisakusho Co., Ltd. at temperatures of 200, 240, 280, and 320°C, which were in accord with the cylinder temperatures in injection molding. The dies used were three straight dies with radius R = 0.25 mm, length L = 1.0, 2.5, and 5.0 mm, and L/R = 4, 10, and 20.

The apparent shear rate $\dot{\gamma}'_w$, the true shear rate $\dot{\gamma}_w$, and the effective shear stress τ_w at the wall in the capillary flow of a viscoelastic fluid are given by eqs. (10), (11), and (12), respectively:

$$\dot{\gamma}'_w = \frac{4Q}{\pi R^3} \quad (10)$$

$$\dot{\gamma}_w = \frac{\dot{\gamma}'_w}{4}\left(3 + \frac{d \log \dot{\gamma}'_w}{d \log \tau_w}\right) \quad (11)$$

$$\tau_w = \frac{(P - P_c - P_e)R}{2L} \quad (12)$$

$$= \frac{PR}{2(L + n_c R + eR)} \quad (12')$$

$$= \frac{PR}{2(L + \nu R)} \quad (12'')$$

$$\nu = n_c + e \quad (13)$$

where P_c and P_e are the pressure loss caused by the contraction of flow at the capillary inlet and the pressure loss caused by the elastic deformation, respectively. $n_c R$ and eR are capillary lengths corresponding to P_c and P_e, respectively, and n_c is the Couette's correction term. According to Philippoff and Gaskins,[67] $2e$ is equal to the recoverable shear strain γ_e(entrance). Namely,

$$\nu = n_c + \frac{\gamma_e(\text{entrance})}{2} \quad (14)$$

Rearranging eq. (12″),

$$P = 2\tau_w(L/R) + 2\nu\tau_w \quad (15)$$

A rectilinear relationship should be obtained if pressure P needed to produce a definite shear stress τ_w and hence a definite shear rate $\dot{\gamma}'_w$ is plotted against L/R (Bagley plot[68]), and the end correction

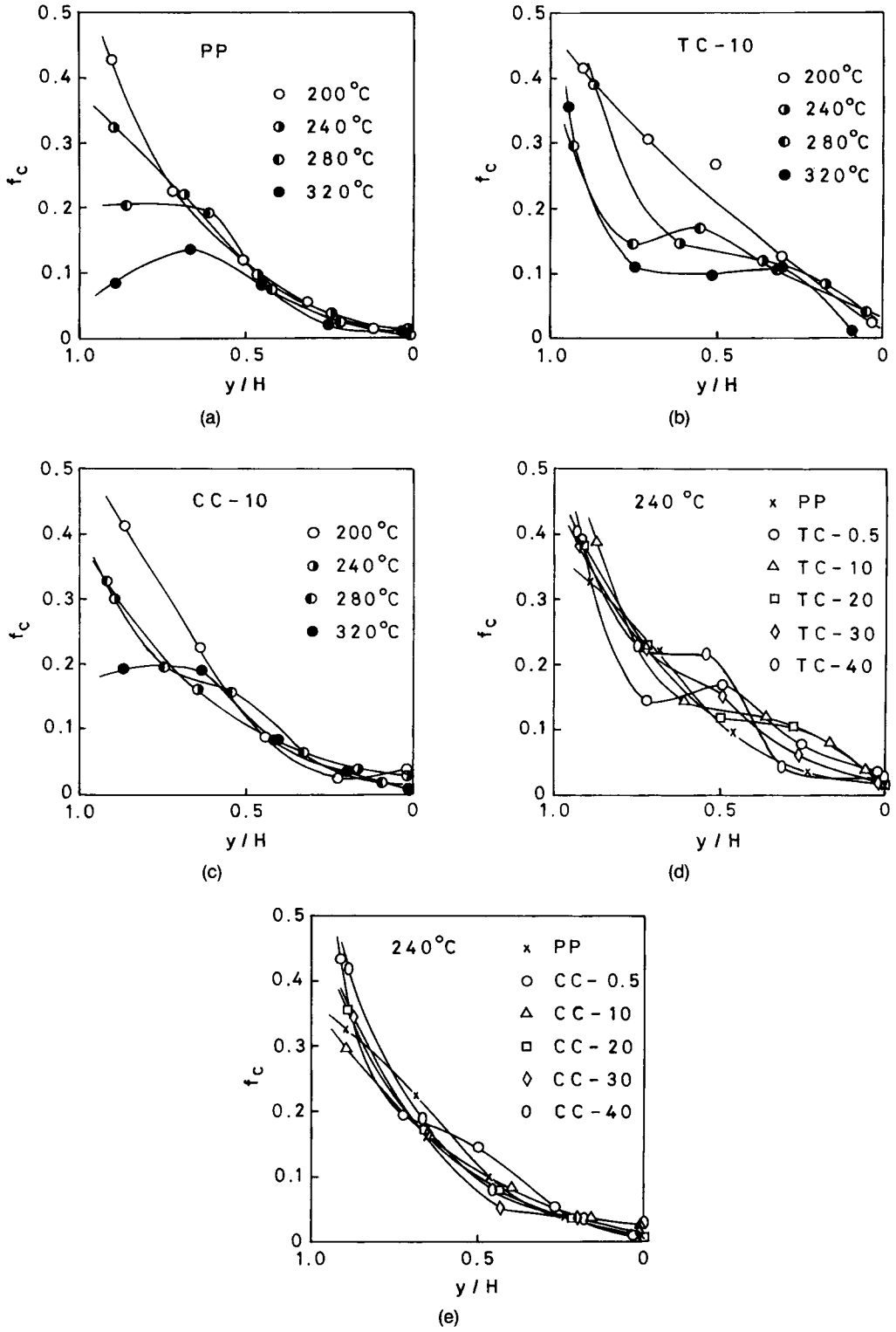

Figure 22 Distribution of c-axis orientation function f_c in thickness direction. (a) PP molded at various cylinder temperatures (b) TC-10 molded at various cylinder temperatures. (c) CC-10 molded at various cylinder temperatures. (d) TC series molded at 240°C. (e) CC series molded at 240°C.

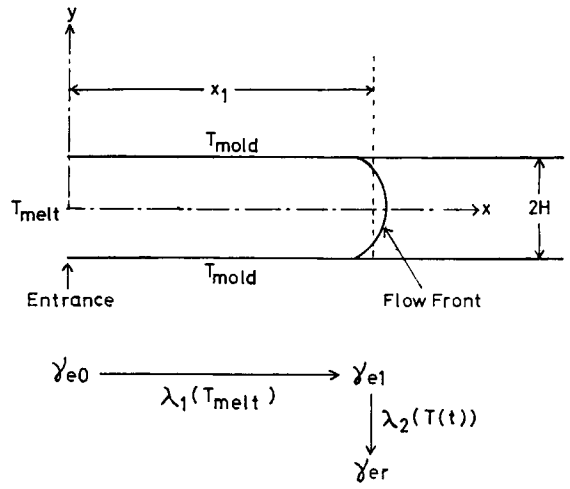

Figure 23 Coordinates and movements of recoverable shear strain γ_e in mold cavity.

coefficient ν is obtained as an intercept of the L/R axis.

γ_e(transient) was obtained as follows: The true shear rate $\dot{\gamma}_w$ and the effective shear stress τ_w were calculated by eqs. (11) and (12), respectively, and the shear viscosity $\eta(\dot{\gamma}_c)$ was calculated by $\eta(\dot{\gamma}_c) = \tau_w/\dot{\gamma}_w$. γ_e(transient) was calculated by eqs. (9) and (8) from $\eta(\dot{\gamma}_c)$, the zero-shear viscosity η_0, and the zero-shear relaxation time γ_0. Since the determination of precise values of η_0 and λ_0 was difficult for samples with high filler contents as shown in the following section and since their values scarcely influenced γ_e(transient) as shown later in Experimental Results section, their approximate values were used for the calculation of γ_e(transient).

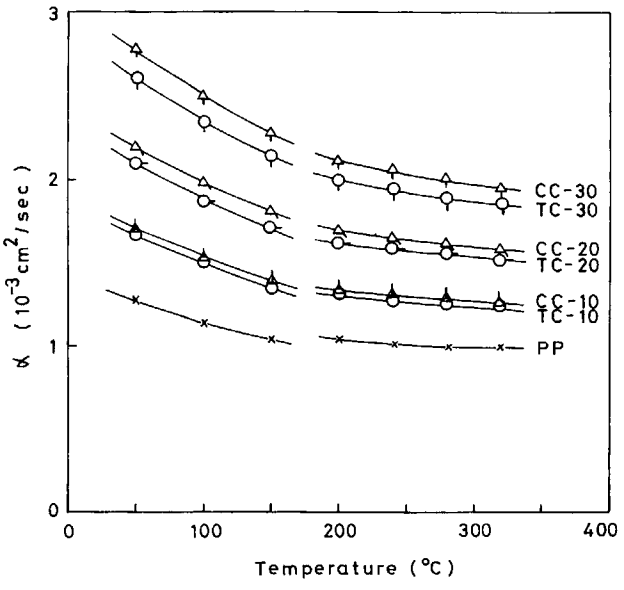

Figure 24 Temperature changes of thermal diffusivity α of particulate-filled polypropylenes.

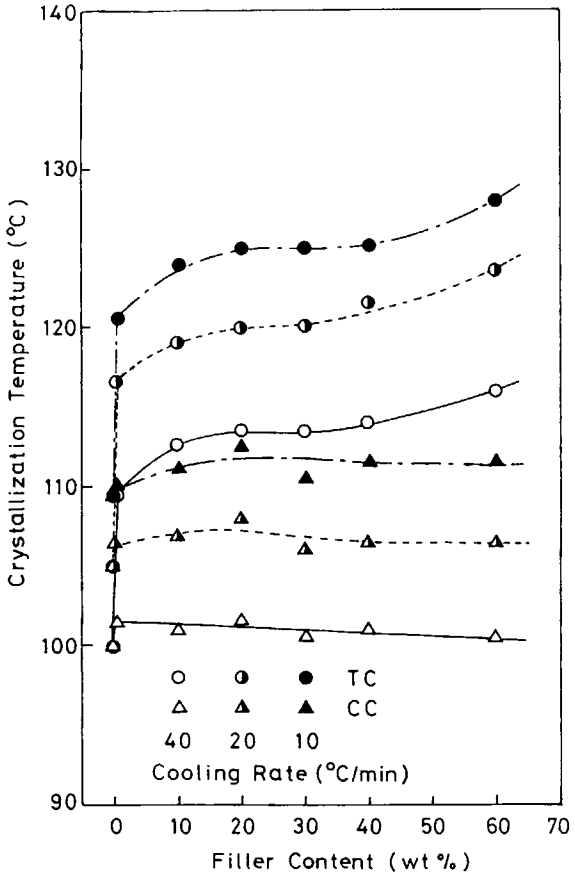

Figure 25 Dependences of crystallization temperature T_c on filler content.

Relaxation Time. The relaxation time λ was obtained from the absolute value of complex viscosity, $|\eta^*(\omega)|$, according to Graessley's method.[69] Graessley showed experimentally that, regardless of the type of polymer and temperature, there is a relationship of

$$\dot{\gamma}_0\eta_0 J_e^0 = 0.6 \pm 0.2 \qquad (16)$$

among $\dot{\gamma}_0$, the shear rate at which the shear viscosity $\eta(\dot{\gamma})$ lowers to 0.8 times the zero-shear viscosity η_0, and η_0 and the steady-state shear compliance J_e^0. Since $\eta(\dot{\gamma})$ and $|\eta^*(\omega)|$ are equivalent functions in a range of low $\dot{\gamma}$ and ω,[70] the characteristic relaxation time $\lambda_0 = \eta_0 J_e^0$ can be calculated, using ω_0, the angular frequency at the time when $|\eta^*(\omega)|$ is $0.8\eta_0$, in place of $\dot{\gamma}_0$ in eq. (16). There were cases at high filler contents where the decrease of $|\eta^*(\omega)|$ with increasing ω occurred in two steps or $|\eta^*(\omega)|$ con-

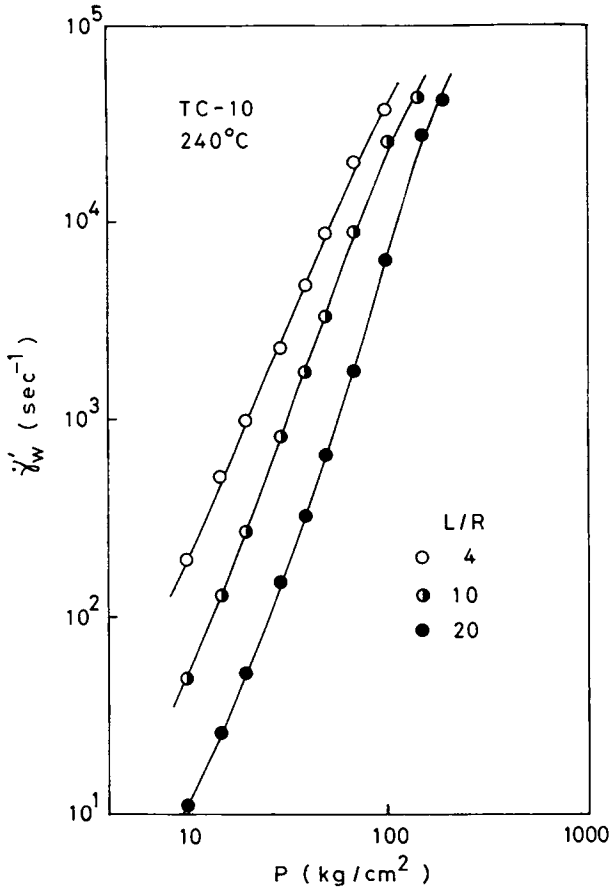

Figure 26 Apparent flow curves measured with dies of various L/R, expressed in the form of apparent shear rate $\dot{\gamma}'_w$ vs. pressure P. TC-10 measured at 240°C.

tinued to increase with decreasing ω, and hence the determination of η_0 was difficult. However, since Bretas and Powell[71] showed that the relaxation time of shear stress of a low density polyethylene filled

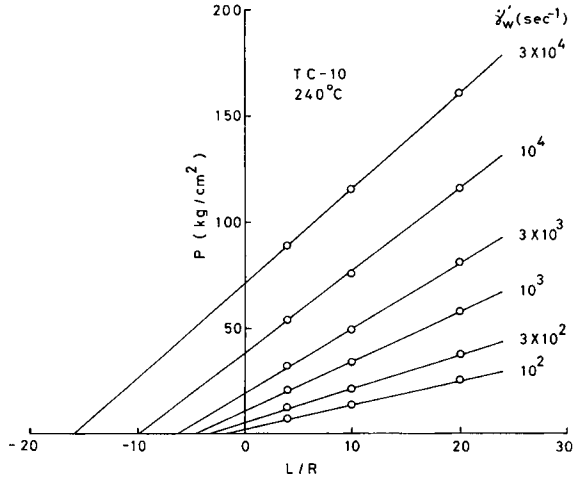

Figure 27 Bagley plots; TC-10; 240°C.

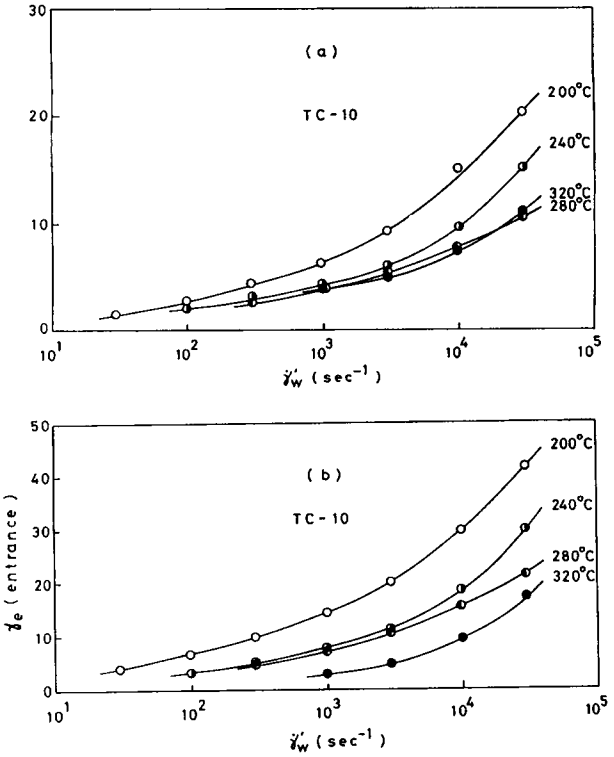

Figure 28 (a) End correction coefficient ν vs. apparent shear rate $\dot{\gamma}'_w$. (b) Entrance component of recoverable shear strain, γ_e (entrance) vs. apparent shear rate $\dot{\gamma}'_w$. TC-10.

with 40 wt % glass beads scarcely changed from that of unfilled one, we assume that the relaxation times of recoverable shear strain of TC- or CC-filled polypropylene melts do not change from that of the unfilled one in the present experiment. Namely, we

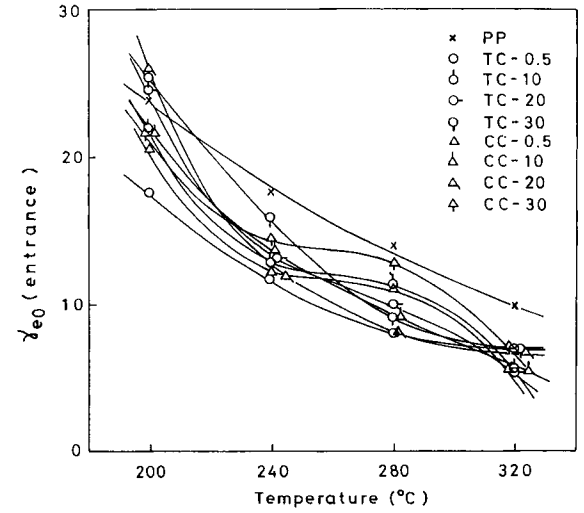

Figure 29 Temperature changes of entrance component of initial recoverable shear strain, γ_{e0} (entrance).

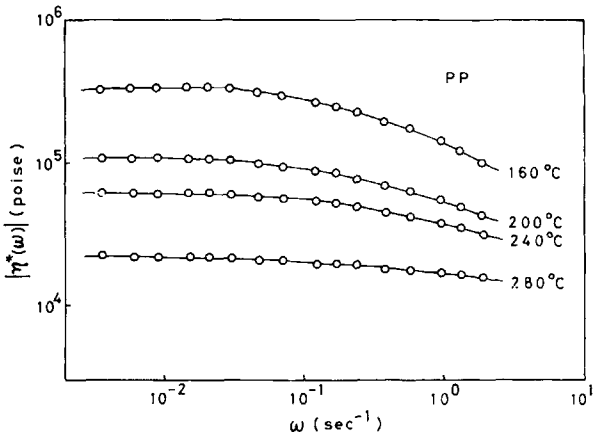

Figure 30 Absolute values of complex viscosities, $|\eta^*(\omega)|$, of PP at various temperatures.

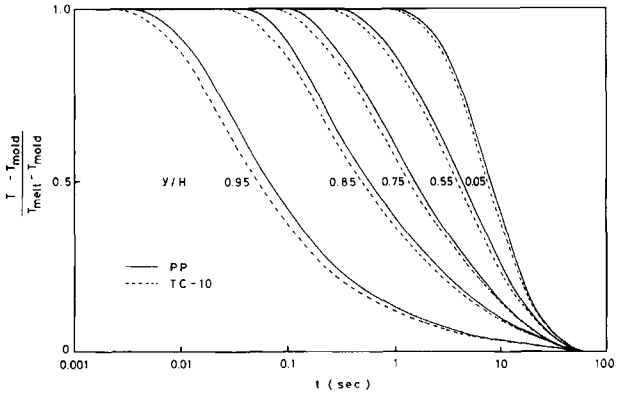

Figure 32 Variations of resin temperatures T of PP and TC-10 at various thicknesswise positions y/H with time t.

regard the relaxation times of recoverable shear strain of TC or CC series as identical to that of PP. Equation (16) shows that there is a standard deviation of ±0.2 depending on the kind of polymer. However, here, 0.6 was used for the right-hand side term of eq. (16) since the subject was only polypropylene.

Measurements of Thermal Properties

Thermal Diffusivity. Thermal diffusivity α was obtained by calculation from document data. For thermal conductivity k of polypropylene, a constant value of 5.0×10^{-4} cal/cm s °C was used for both solid and molten states according to Matsumoto et al.'s solid-state value of 4.5×10^{-4} cal/cm s °C[72] and Fuller and Fricke's molten-state value of 5.0×10^{-4} cal/cm s °C.[73] Density ρ of polypropylene was calculated from Danusso et al.'s empirical formulae concerning the temperature changes of specific volumes v_c and v_a of, respectively, crystalline and amorphous polypropylenes.[74] Specific heat C_p of polypropylene was calculated from Gee and Melia's empirical formulae.[75]

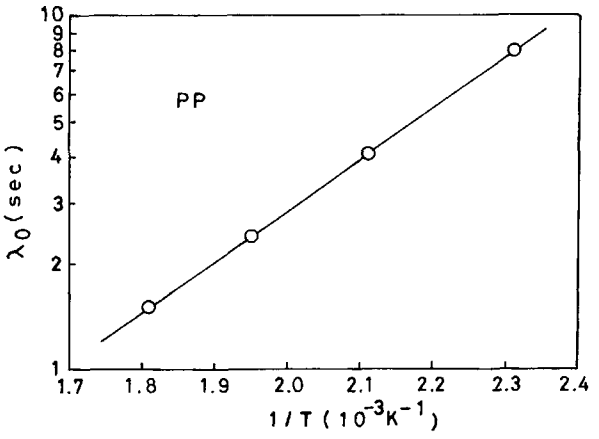

Figure 31 Arrhenius plot of characteristic relaxation time λ_0 of PP.

Characteristic values of fillers were taken from the handbook of Katz and Milewski.[76] Namely, k's of TC and CC were 5.0×10^{-3} and 5.6×10^{-3} cal/cm s °C, respectively, C_p's of TC and CC were 0.208 and 0.21 cal/°C g, respectively, and ρ's of TC and CC were 2.7 g/cm^3.

k's, C_p's, and ρ's of particulate-filled polypropylenes were calculated by use of volumetric additivities of k, C_p, and specific volume v,[76] respectively. Thermal diffusivity α was calculated from k, ρ, and C_p by $\alpha = k/\rho C_p$.

The temperature changes of α calculated in this way are shown in Figure 24. α increases by particulate filling. The values of α do not greatly change at temperatures encountered by a resin in injection molding. Therefore, values at 200°C were used for calculations in orientation analysis.

Crystallization Temperature. A thermogram was measured with a sheet about 0.3 mm thick at cooling rates of 10, 20, and 40°C/min using a differential scanning calorimeter, Perkin Elmer DSC-BI, after melting for 10 min at 230°C in nitrogen gas flow, and the exothermic peak was taken as crystallization temperature T_c. The results are shown in Figure 25. T_c is greatly increased by TC filling of a small amount of 0.5 wt % and gradually increases after that with increasing TC content. T_c is increased by 1–2°C by CC filling and scarcely depends on CC content. It can be said from these results that TC has a strong crystallization nucleation ability and CC has almost no nucleation ability. T_c's

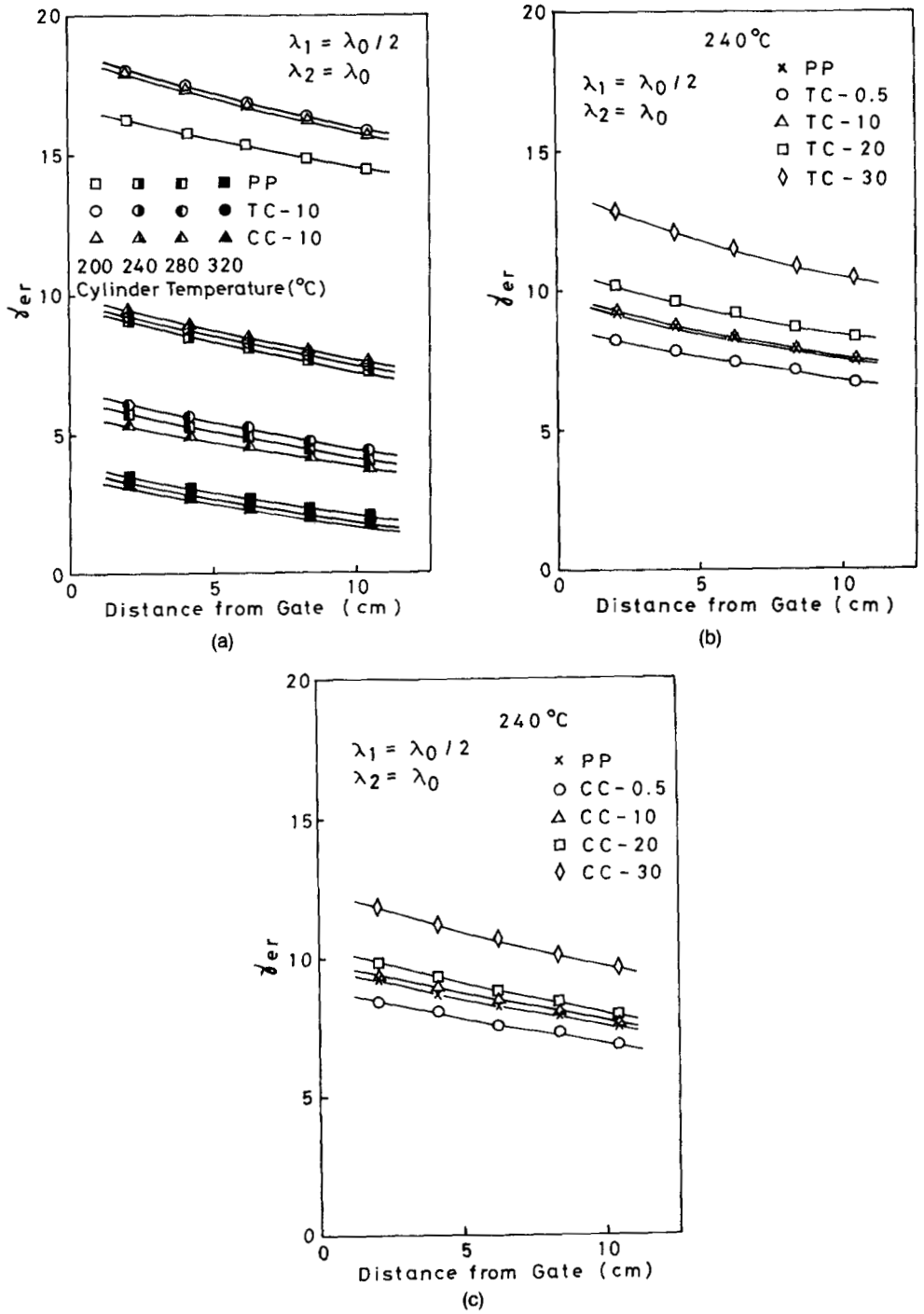

Figure 33 Distribution of calculated mean residual recoverable shear strain γ_{er} in flow direction. $\lambda_1 = \lambda_0/2$, $\lambda_2 = \lambda_0$. (a) PP, TC-10, and CC-10 molded at various cylinder temperatures. (b) TC series molded at cylinder temperature of 240°C. (c) CC series molded at cylinder temperature of 240°C.

decrease with increasing cooling rate. For calculations in the analysis of orientation process, T_c's at a cooling rate of 40°C/min were used in consideration of the high cooling rate met in injection molding.

Experimental Results

Recoverable Shear Strain

Figure 26 exemplifies apparent flow curves expressed in the form of the apparent shear rate $\dot{\gamma}'_w$ vs. pressure

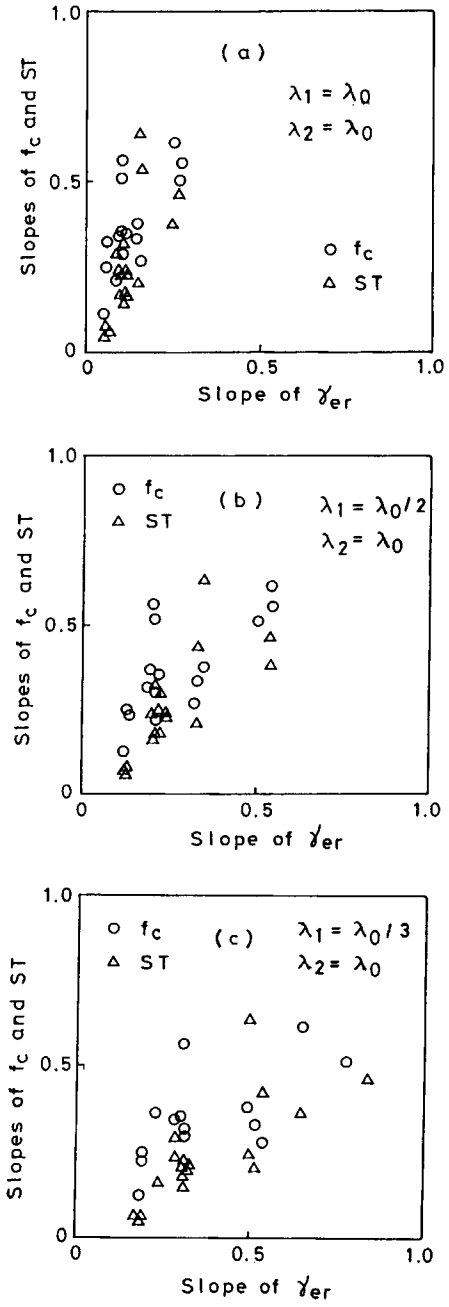

Figure 34 Plots of slopes of c-axis orientation function f_c and thickness of skin layer, ST, in flow direction vs. slope of calculated mean residual recoverable shear strain γ_{er} in flow direction: (a) $\lambda_1 = \lambda_0$; (b) $\lambda_1 = \lambda_0/2$; (c) $\lambda_1 = \lambda_0/3$.

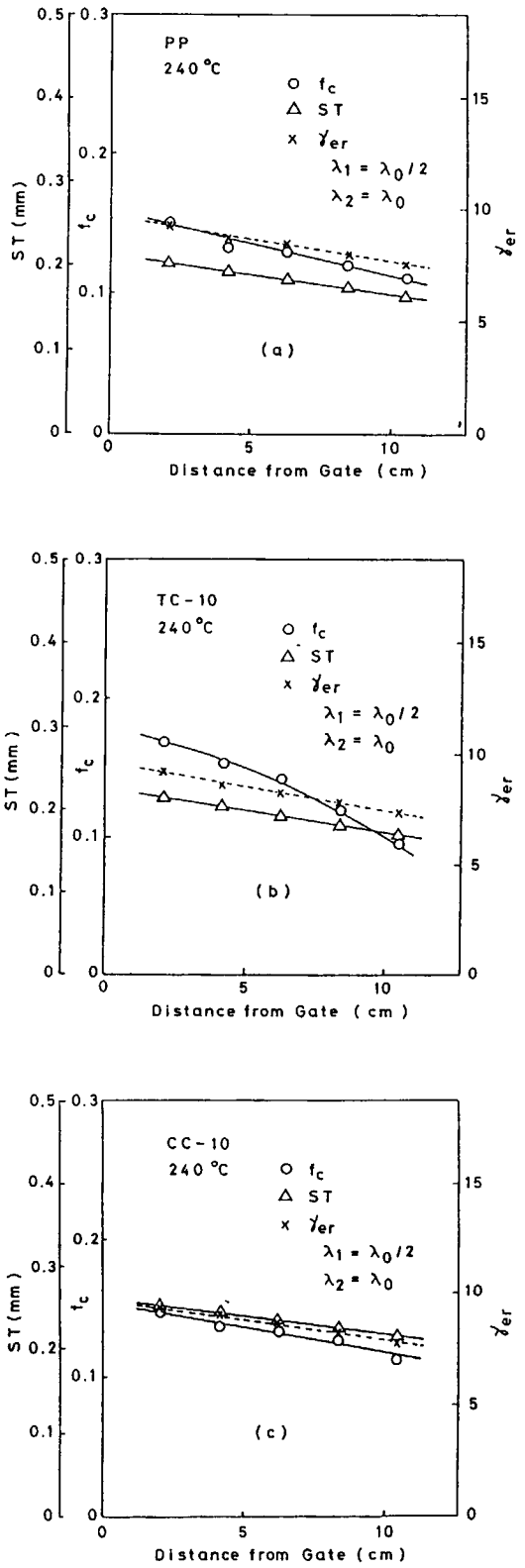

Figure 35 Variations in flow direction, of c-axis orientation function f_c, thickness of skin layer, ST, and calculated mean residual recoverable shear strain γ_{er}: (a) PP, (b) TC-10, and (c) CC-10 molded at a cylinder temperature of 240°C.

P, of TC-10 measured at 240°C using various L/R dies. The Bagley plots carried out, using Figure 26, are shown in Figure 27. Fine Bagley plots were obtained for all samples at all temperatures.

Figure 28(a) exemplifies the change with $\dot{\gamma}'_w$ of the end correction coefficient ν obtained with Bagley plots for TC-10. ν tends to decrease as temperature

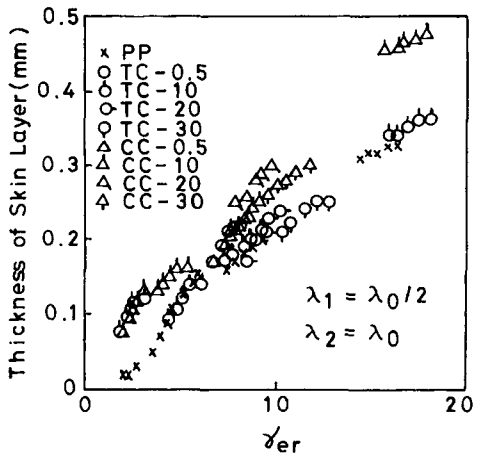

Figure 36 Relation between thickness of skin layer and calculated mean residual recoverable shear strain γ_{er} at various positions in flow direction: $\lambda_1 = \lambda_0/2$, $\lambda_2 = \lambda_0$.

rises. A similar tendency was obtained with all other samples.

According to Bagley,[77] Hook's law of the following expression holds:

$$\tau_w = \mu\gamma_e(\text{entrance}) \qquad (17)$$

where τ_w is shear stress, μ is the shear modulus, and γ_e(entrance) is the entrance component of recoverable shear strain.

If eq. (17) is substituted into eq. (14),

$$\nu = \frac{\tau_w}{2\mu} + n_c \qquad (18)$$

Therefore, if the end correction coefficient ν is plotted against shear stress τ_w, a rectilinear relationship should be obtained and the Couette's correlation term n_c is obtained from an intercept of the ν-axis. The recoverable shear strain γ_e(entrance) was obtained by substituting into eq. (14) n_c, which had been obtained by plotting ν against τ_w and extrapolating τ_w into 0, where the effective shear stress τ_w had been calculated by eq. (12″) using ν, which had been obtained from the Bagley plots. Figure 28(b) exemplifies the change of γ_e(entrance) with $\dot{\gamma}'_w$ for TC-10. γ_e(entrance) increases with increasing $\dot{\gamma}'_w$ and decreases as temperature rises. A similar tendency was observed with all other samples.

Apparent shear rate $\dot{\gamma}'_w$ at the wall in slit flow is given by the following equation[78]:

$$\dot{\gamma}'_w = \frac{6Q}{(2H)^2(B + 2H)} \qquad (19)$$

where Q is the volumetric flow rate, $2H$ is the thickness of the slit, and B is its width. If the shear rate at the gate in injection molding under this experiment is calculated using eq. (19), $\dot{\gamma}'_w \fallingdotseq 4200\ s^{-1}$. Then, γ_e(entrance) at $\dot{\gamma}'_w = 4200\ s^{-1}$ can be taken as the initial recoverable shear strain γ_{e0}(entrance) mentioned in the previous section. The temperature change of γ_{e0}(entrance) is shown in Figure 29. γ_{e0}(entrance) tends to decrease with increasing temperature and by particulate filling.

On the other hand, the transient component of recoverable shear strain, γ_{e0}(transient), was calculated using eqs. (8) and (9). It scarcely depended on the kind of resin and temperature and had a value of about 9.2. Then, total initial recoverable shear strain γ_{e0} was obtained by the following equation:

$$\gamma_{e0} = \gamma_{e0}(\text{entrance}) + \gamma_{e0}(\text{transient}) \qquad (20)$$

Relaxation Time

Figure 30 shows the temperature change of the absolute value of complex viscosity, $|\eta^*(\omega)|$, of PP. It is seen that behaviors of from Newtonian flow to non-Newtonian flow appear.

Figure 31 shows the temperature change of the characteristic relaxation time λ_0, which was obtained by Graessley's method. λ_0 obeys the Arrhenius equation and is expressed by

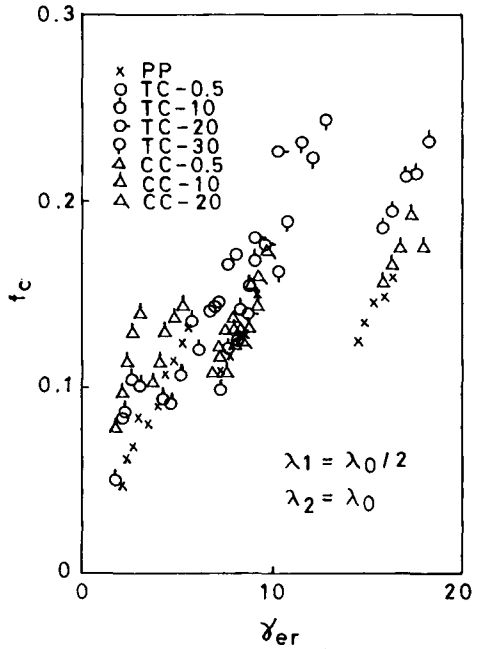

Figure 37 Relation between c-axis orientation function f_c and calculated mean residual recoverable shear strain γ_{er} at various positions in flow direction: $\lambda_1 = \lambda_0/2$, $\lambda_2 = \lambda_0$.

$$\lambda_0 = 3.49 \times 10^{-3} \exp\left(\frac{3340}{T + 273}\right) \quad (21)$$

Therefore, $\lambda_1(T)$ and $\lambda_2(T)$ mentioned in the Theory section are given in the forms of

$$\lambda_1(T) = A\lambda_0 = 3.49 \times 10^{-3} A \exp\left(\frac{3340}{T + 273}\right) \quad (22)$$

$$\lambda_2(T) = B\lambda_0 = 3.49 \times 10^{-3} B \exp\left(\frac{3340}{T + 273}\right) \quad (23)$$

where A and B are constants independent of temperature.

Analysis of Molecular Orientation Process

Figure 32 exemplifies the changes of resin temperatures T of PP and TC-10 with position in the thickness direction, y/H, and time t, calculated by eq. (5). Here, T is expressed by a nondimensional quantity of $(T - T_{mold})/(T_{melt} - T_{mold})$. As a matter of course, cooling rate is higher nearer the surface of large y/H. The fact that the cooling rate of TC-10 is higher than that of PP is because the thermal diffusivity α of the former is higher than that of the latter. The cooling rate increases with increasing filler content since α increases with increasing filler content as shown in Figure 24.

The shear rate in the mold cavity, calculated by eq. (19), is about 500 s^{-1}, which means that flow in the mold cavity is sufficiently in the nonlinear region. Since there is possibility that the relaxation time in nonlinear flow is shorter than the relaxation time in linear flow region, λ_0,[79] at first, we will evaluate the relaxation time in cavity flow, λ_1. Assuming that $\lambda_2 = \lambda_0$, the change of residual recoverable shear strain γ_{er} in the flow direction when $\lambda_1 = \lambda_0$, $\lambda_0/2$, and $\lambda_0/3$ was calculated using eqs. (5), (7), (22), and (23). Figures 33(a)–(c) exemplify the calculation results when $\lambda_1 = \lambda_0/2$. From these, the slopes of γ_{er} are calculated by

$$\text{slope of } \gamma_{er} = \frac{\gamma_{er}(2.1) - \gamma_{er}(10.5)}{\gamma_{er}(6.3)} \quad (24)$$

where $\gamma_{er}(2.1)$, $\gamma_{er}(6.3)$, and $\gamma_{er}(10.5)$ are the recoverable shear strains at the positions 2.1, 6.3, and 10.5 cm far from the gate, respectively. Next, by the same manner as in the case of γ_{er}, the slopes of the changes in the flow direction, of the thickness of the skin layer, ST, and the crystalline c-axis orientation function f_c are calculated from the changes of ST in the flow direction in Figure 13 and the changes of f_c in the flow direction in Figure 16, respectively:

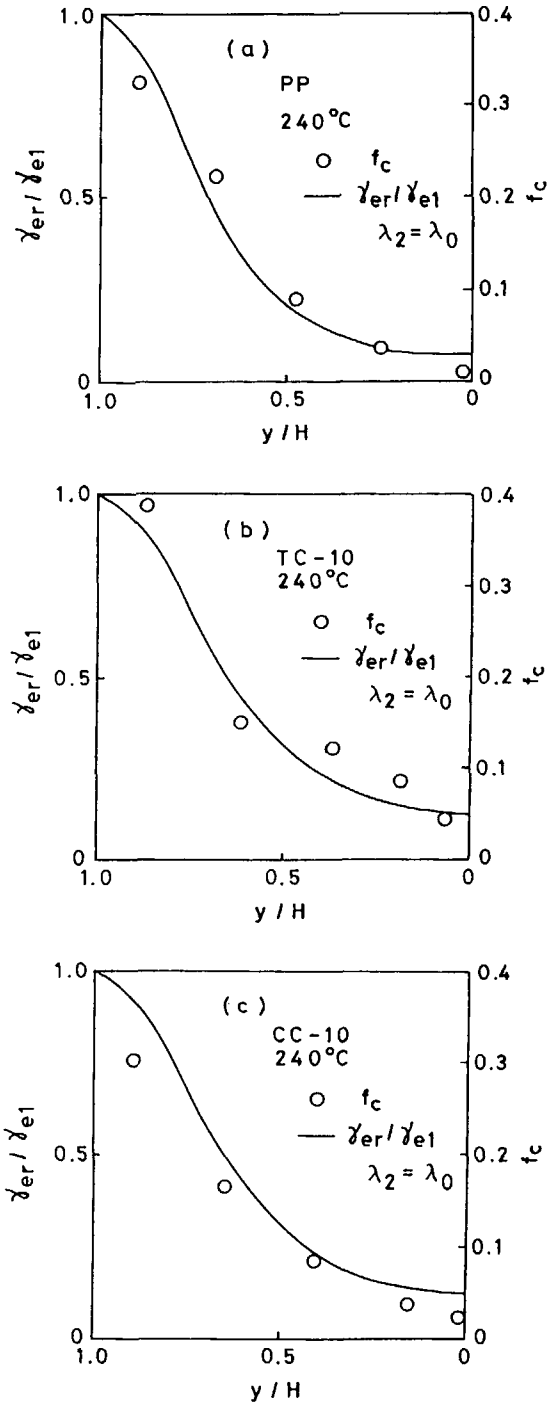

Figure 38 Variations with thicknesswise position y/H, of c-axis orientation function f_c and calculated relative residual recoverable shear strain γ_{er}/γ_{e1}: (a) PP, (b) TC-10, and (c) CC-10 molded at cylinder temperature of 240°C.

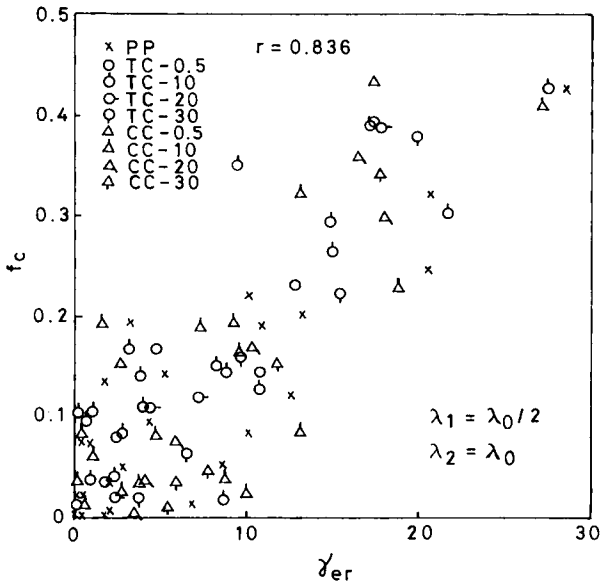

Figure 39 Relation between c-axis orientation function f_c and calculated residual recoverable shear strain γ_{er} at various positions in thickness direction: $\lambda_1 = \lambda_0/2$, $\lambda_2 = \lambda_0$. Data points $n = 90$; correlation coefficient $r = 0.836$.

$$\text{slope of ST} = \frac{\text{ST}(2.1) - \text{ST}(10.5)}{\text{ST}(6.3)} \quad (25)$$

$$\text{slope of } f_c = \frac{f_c(2.1) - f_c(10.5)}{f_c(6.3)} \quad (26)$$

Next, the slopes of ST and f_c are plotted against the slope of γ_{er}. These plots are shown in Figure 34, which shows that the slope of correlation is larger than unity when $\lambda_1 = \lambda_0$, the slope is smaller than unity when $\lambda_1 = \lambda_0/3$, and the slopes of measured degrees of molecular orientation such as ST and f_c and that of calculated residual recoverable shear strain γ_{er} are in a proportional relationship with a slope of about unity when $\lambda_1 = \lambda_0/2$. It is conjectured from these results that the relaxation time of recoverable shear strain, λ_1, at the shear rate of 500 s^{-1} in the cavity flow in this experiment is about a half of the characteristic relaxation time in linear flow, λ_0. Accordingly, $\lambda_0/2$ is used as λ_1 in the following calculations.

Figures 35(a)-(c) exemplify how the c-axis orientation functions f_c, the thicknesses of the skin layer, ST, and the calculated mean residual recoverable shear strains γ_{er} change in the flow direction for flexural specimens molded from, respectively, PP, TC-10, and CC-10 at a cylinder temperature of 240°C. ST and f_c decrease in proportion to the distance from the gate and the degrees of these decreases are nearly the same as that of γ_{er}. Similar results were obtained for specimens molded from other samples at other cylinder temperatures.

Figures 36 and 37 show relations between, respectively, the thickness of the skin layer and the c-axis orientation function f_c, and the calculated mean residual recoverable shear strain γ_{er}, at various positions in the flow direction of specimens molded from various samples at various cylinder temperatures. Fairly high correlations exist between the two.

Figures 38(a)-(c) exemplify comparisons between the changes in the thickness direction of the c-axis orientation functions f_c and the relative residual recoverable shear strains γ_{er}/γ_{e1} calculated using eqs. (5), (6), and (23), for specimens molded from, respectively, PP, TC-10, and CC-10 at a cylinder temperature of 240°C. The two agree well, thus showing the propriety of using the characteristic relaxation time λ_0 as the relaxation time of recoverable shear strain after cessation of flow in the mold cavity, λ_2.

Figure 39 shows the relation between the c-axis orientation function f_c and calculated residual recoverable shear strain γ_{er} at various positions in the thickness direction of specimens molded from various samples at various cylinder temperatures. Data points n are 90. A fairly high correlation with a correlation coefficient $r = 0.836$ exists between the two.

Figures 40 and 41 show the relation between, respectively, the thickness of the skin layer and the c-axis orientation function f_c and the calculated mean residual recoverable shear strain γ_{er}, at the

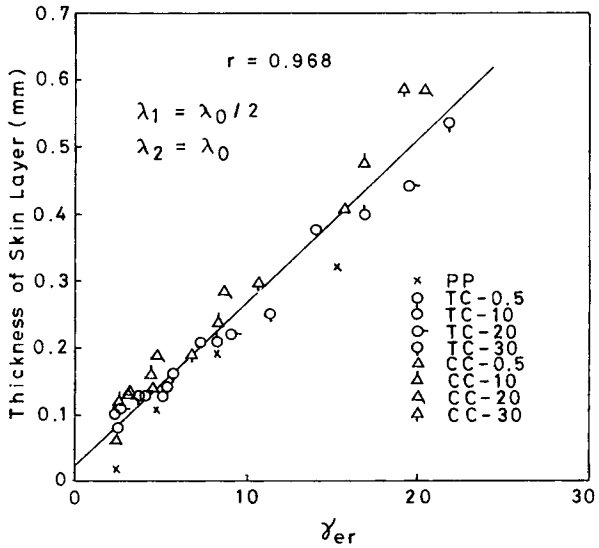

Figure 40 Relation between thickness of skin layer and calculated mean residual recoverable shear strain γ_{er}: $\lambda_1 = \lambda_0/2$, $\lambda_2 = \lambda_0$.

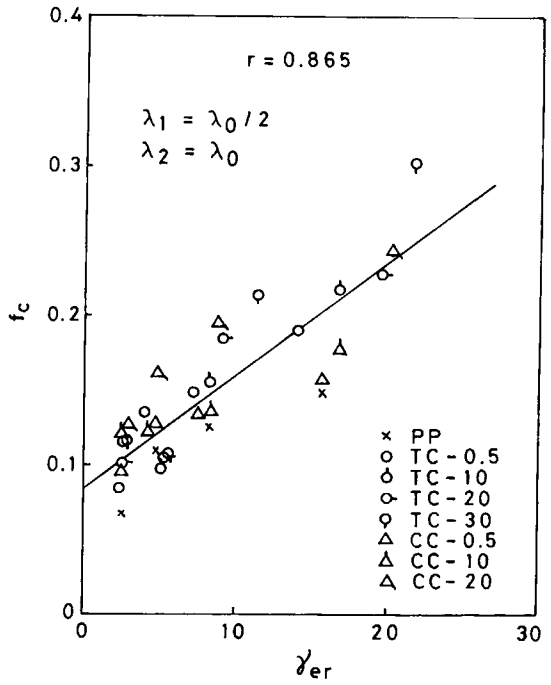

Figure 41 Relation between c-axis orientation function f_c and calculated mean residual recoverable shear strain γ_{er}: $\lambda_1 = \lambda_0/2$, $\lambda_2 = \lambda_0$.

centers of flexural specimens molded from various samples at various cylinder temperatures. Between the two, fairly high correlations exist regardless of the kind and content of filler and molding conditions (cylinder temperature).

As mentioned above, this theory can considerably well describe not only the mean molecular orientation but also its change in the flow and thickness directions in injection moldings of particulate-filled polypropylenes.

CONCLUSIONS

Flexural test specimens were injection-molded from polypropylenes filled with flaky talc (TC) or spherical calcium carbonate (CC) at levels of 0–40 wt % under cylinder temperatures of 200–320°C and distributions of higher-order structures in the flow and thickness directions were studied.

Distribution of Higher-Order Structures in Flow Direction

(i) The thickness of the skin layer is higher as filler content is higher and cylinder temperature is lower and decreases with going away from the gate.

(ii) a^*-Axis-oriented component fraction $[A^*]$ is higher as cylinder temperature is higher and increases a little with going away from the gate. Although CC filling scarcely influences $[A^*]$, TC filling decreases $[A^*]$.

(iii) The crystalline c-axis orientation function f_c is higher as filler content is higher and cylinder temperature is lower and decreases with going away from the gate.

Distribution of Higher-Order Structures in Thickness Direction

(i) Crystallinity X_c is low at the surface region and increases toward the interior. Although CC filling scarcely influences X_c, TC filling increases X_c.

(ii) The β-crystals exist at the surface region of about twice the thickness of the skin layer and do not exist at the inner region. While TC filling decreases β-crystal content, CC filling increases β-crystal content.

(iii) The degree of b-axis orientation to the thickness direction is somewhat low near the surface region, increases once, and decreases toward the interior for PP. Although CC filling scarcely influences the b-axis orientation, TC filling strongly increases the b-axis orientation across almost the whole range in the thickness direction. The b-axis orientation strongly appears already by the TC filling of only 0.5 wt %.

(iv) $[A^*]$ is low at the surface region and increases toward the interior for PP. Although CC filling scarcely influences $[A^*]$, TC filling greatly decreases $[A^*]$. $[A^*]$'s of TC-filled polypropylenes decrease toward the interior.

(v) f_c is high at the surface region and decreases toward the interior. f_c at the surface region is higher as cylinder temperature is lower. There are cases where peaks or shoulders of f_c are observed at midway regions in the thickness direction at high cylinder temperatures, which are assumed to be caused by the secondary flow during the cooling and pressure holding process. TC or CC filling scarcely influences f_c.

Analysis of Molecular Orientation Process

A theoretical analysis of molecular orientation in injection molding was made from a viewpoint of growth of a recoverable shear strain at the gate and

its relaxation in the cavity and could considerably well describe the influences of particulate filling and cylinder temperature on not only the mean values but also the changes in the flow and thickness directions, of quantities such as the thickness of the skin layer and the crystalline c-axis orientation function f_c, which express the degree of molecular orientation.

The authors would like to thank Tokuyama Soda Co., Ltd. for permission to publish this paper.

REFERENCES

1. P. F. Folks and D. A. M. Russell, *Polymer,* **21,** 1252 (1980).
2. S. F. Xavier, D. Tyagi, and A. Misra, *Polym. Compos.,* **3,** 88 (1982).
3. S. F. Xavier and A. Misra, *Polym. Compos.,* **6,** 93 (1985).
4. R. H. Burton and M. J. Folks, *Plast. Rubber Process. Appl.,* **3,** 129 (1983).
5. A. Misra, B. L. Deopura, S. F. Xavier, F. D. Hartley, and R. H. Peters, *Angew. Makromol. Chem.,* **113,** 113 (1983).
6. S. F. Xavier and Y. N. Sharma, *Angew. Makromol. Chem.,* **127,** 145 (1984).
7. R. H. Burton, T. M. Day, and M. J. Folks, *Polym. Commun.,* **25,** 361 (1984).
8. C. Lhymn and J. M. Shultz, *Polym. Compos.,* **6,** 87 (1985).
9. S. F. Xavier and Y. N. Sharma, *Polym. Compos.,* **7,** 42 (1986).
10. M. Fujiyama, Y. Kawasaki, and T. Wakino, *Nihon Reoroji Gakkaishi,* **15,** 191 (1987).
11. M. Fujiyama, Y. Kawasaki, and T. Wakino, *Nihon Reoroji Gakkaishi,* **15,** 203 (1987).
12. E. Morales and J. R. White, *J. Mater. Sci.,* **23,** 3612 (1988).
13. M. R. Kamal, L. Song, and P. Singh, *SPE Tech. Pap. 44th ANTEC,* **32,** 133 (1986).
14. R. K. Bayer, T. A. Ezquerra, H. G. Zachmann, F. J. B. Calleja, J. M. Salazar, W. Meins, R. E. Diekow, and P. Wiegel, *J. Mater. Sci.,* **23,** 475 (1988).
15. T. A. Ezquerra, R. K. Bayer, and F. J. B. Calleja, *J. Mater. Sci.,* **23,** 4121 (1988).
16. M. Fujiyama and T. Wakino, *J. Appl. Polym. Sci.,* **42,** 9 (1991).
17. M. Fujiyama and S. Kimura, *Kobunshi Ronbunshu,* **32,** 581 (1975).
18. Z. W. Wilchinsky, *J. Appl. Phys.,* **31,** 1969 (1960).
19. W. Weidinger and P. H. Hermans, *Makromol. Chem.,* **50,** 98 (1961).
20. A. Turner-Jones, J. M. Aizilewood, and D. R. Beckert, *Makromol. Chem.,* **75,** 134 (1964).
21. F. Altendorfer and E. Seitl, *Plastverarbeiter,* **35,** 144 (1984).
22. A. Krsova, *Int. Polym. Sci. Tech.,* **4**(10), T/33 (1977).
23. H. Hirose, K. Ito, and T. Kawano, *Plast. Jpn.,* **26**(2), 13 (1980).
24. F. Altendorfer and G. Geymayer, *Plastverarbeiter,* **34,** 511 (1983).
25. F. Altendorfer and E. Seitl, *Kunststoffe,* **76,** 47 (1986).
26. J. Koppelmann, E. Fleischmann, and G. Leiter, *Rheol. Acta,* **26,** 548 (1987).
27. E. Fleischmann and J. Koppelmann, *Kunststoffe,* **78,** 453 (1988).
28. G. Menges, H. Ries, and T. Wiegmann, *Kunststoffe,* **77,** 917 (1987).
29. M. Fujiyama and T. Wakino, *J. Appl. Polym. Sci.,* **43,** 57 (1991).
30. J. P. Trotignon, J. L. Lebrun, and J. Verdu, *Plast. Rubber Process. Appl.,* **2,** 247 (1982).
31. J. P. Trotignon and J. Verdu, *J. Appl. Polym. Sci.,* **34,** 1 (1987).
32. J. P. Trotignon and J. Verdu, *J. Appl. Polym. Sci.,* **34,** 19 (1987).
33. M. W. Murphy, K. Thomas, and M. J. Bevis, *Plast. Rubber Process. Appl.,* **9,** 3 (1988).
34. M. W. Murphy, K. Thomas, and M. J. Bevis, *Plast. Rubber Process. Appl.,* **9,** 117 (1988).
35. G. Menges, A. Troost, J. Koske, H. Ries, and H. Stabrey, *Kunststoffe,* **78,** 806 (1988).
36. S. Kubota, *Polym. Prepr. Jpn.,* **36,** 3677 (1987).
37. M. Houska and M. Brummell, *Polym. Eng. Sci.,* **27,** 917 (1987).
38. M. Houska and M. Brummell, *Plaste Kautschuk,* **35,** 83 (1988).
39. M. R. Kantz, H. D. Newman, Jr., and F. H. Stigale, *J. Appl. Polym. Sci.,* **16,** 1249 (1972).
40. D. R. Fitchmun and Z. Mencik, *J. Polym. Sci. Polym. Phys. Ed.,* **11,** 951 (1973).
41. F. H. Moy and M. R. Kamal, *Polym. Eng. Sci.,* **20,** 957 (1980).
42. M. R. Kamal and F. H. Moy, *Polym. Eng. Rev.,* **2,** 381 (1983).
43. M. R. Kamal and F. H. Moy, *J. Appl. Polym. Sci.,* **28,** 1787 (1983).
44. E. Fleischmann and J. Koppelmann, *Kunststoffe,* **77,** 405 (1987).
45. R. L. Ballman and H. L. Toor, *Mod. Plast.,* **38** (Oct.), 113 (1960).
46. J. L. S. Wales, J. Van Leeuwen, and R. Van Der Vijgh, *Polym. Eng. Sci.,* **12,** 358 (1972).
47. G. Menges and G. Wübken, *SPE Tech. Pap. 31st ANTEC,* **19,** 519 (1973).
48. Z. Tadmor, *J. Appl. Polym. Sci.,* **18,** 1753 (1974).
49. E. L. Kalinchev, M. B. Sakovtseva, and E. D. Zhukovskaya, *Int. Polym. Sci. Technol.,* **3**(12), T/29 (1976).
50. H. Janeschitz-Kriegl, *Rheol. Acta,* **16,** 327 (1977).
51. M. Fujiyama and S. Kimura, *J. Appl. Polym. Sci.,* **22,** 1225 (1978).
52. C. D. Han and C. A. Villamizar, *Polym. Eng. Sci.,* **13,** 173 (1978).

53. W. Dietz, J. L. White, and E. S. Clark, *Polym. Eng. Sci.*, **18**, 273 (1978).
54. W. Dietz and J. L. White, *Rheol. Acta*, **17**, 676 (1978).
55. A. I. Isayev and C. A. Hieber, *Rheol. Acta*, **19**, 168 (1980).
56. J. Greener and G. H. Pearson, *J. Rheol.*, **27**, 115 (1983).
57. M. Kohyama, Y. Akane, and T. Okamoto, *Polym. Prepr. Jpn.*, **32**(10), 3089 (1983).
58. P. G. Lafleur and M. R. Kamal, *Polym. Eng. Sci.*, **26**, 92 (1986).
59. M. R. Kamal and P. G. Lafleur, *Polym. Eng. Sci.*, **26**, 103 (1986).
60. M. Fujiyama, *Nihon Reoroji Gakkaishi*, **14**, 152 (1986).
61. H. Mavridis, A. N. Hrymak, and J. Vlachopoulos, *J. Rheol.*, **32**, 639 (1988).
62. J. Greener, R. Kesel, and B. A. Contestable, *AIChE J.*, **35**, 449 (1989).
63. T. Kanai, K. Shimizu, and Y. Uryu, *Int. Polym. Process.*, **4**, 132 (1989).
64. K. Tada, *Fifth Annu. Meeting PPS Prepr.*, 42 (1989).
65. H. S. Carslaw and J. C. Jaeger, *Conduction of Heat in Solid*, 2nd ed., Oxford University Press, Oxford, 1957.
66. H. Heron, S. Pederson, and L. L. Chapoy, *Rheol. Acta*, **15**, 379 (1976).
67. W. Philippoff and F. H. Gaskins, *Trans. Soc. Rheol.*, **2**, 263 (1958).
68. E. B. Bagley, *J. Appl. Phys.*, **28**, 624 (1957).
69. W. W. Graessley, *Adv. Polym. Sci.*, **16**, 1 (1974).
70. W. P. Cox and E. H. Merz, *J. Polym. Sci.*, **28**, 619 (1958).
71. R. E. S. Bretas and R. L. Powell, *Rheol. Acta*, **24**, 69 (1985).
72. T. Matsumoto, T. Watanabe, and T. Hisamoto, *Kogakuin Univ. Res. Rep.*, **52**, 105 (1982).
73. T. R. Fuller and A. L. Fricke, *J. Appl. Polym. Sci.*, **15**, 1729 (1971).
74. F. G. Danusso, G. Maraglio, W. Ghiglia, L. Motta, and G. Talamini, *Chem. Ind.*, **41**, 74 (1959).
75. D. R. Gee and T. P. Melia, *Makromol. Chem.*, **132**, 195 (1970).
76. H. S. Katz and J. V. Milewski, *Handbook of Fillers and Reinforcements for Plastics*, Van Nostrand Reinhold, New York, 1978.
77. E. B. Bagley, *J. Appl. Phys.*, **31**, 1126 (1960).
78. R. B. Staub, *SPE J.*, (Apr.), 429 (1960).
79. M. Sakai, H. Fukaya, and M. Nagasawa, *Trans. Soc. Rheol.*, **16**, 635 (1972).

Received December 18, 1989
Accepted November 9, 1990